Unsymmetrically Substituted Bis(phosphino)Ferrocenes Triggering Through-Space 31 (P, P')-Nuclear Spin Couplings and Encapsulating Coinage Metal Cations

Tuan-Anh Nguyen, Marie-José Penouilh, Hélène Cattey, Nadine Pirio, Paul Fleurat-Lessard, Jean-Cyrille Hierso, Julien Roger

Unsymmetrically Substituted Bis(phosphino)Ferrocenes Triggering Through-Space ^{31}(P, P')-Nuclear Spin Couplings and Encapsulating Coinage Metal Cations

Tuan-Anh Nguyen,[†] Marie-José Penouilh,[†] Hélène Cattey,[†] Nadine Pirio,[†] Paul Fleurat-Lessard,[†] Jean-Cyrille Hierso,*[,†] and Julien Roger*[,†]

[†]Institut de Chimie Moléculaire de l'Université de Bourgogne (ICMUB - UMR CNRS 6302), Université Bourgogne–Franche-Comté (UBFC), 9 avenue Alain Savary, 21078 Dijon Cedex, France

ABSTRACT: We describe unsymmetrically substituted di-*tert*-butylated 1,1'-bis(phosphino)ferrocenes, with phosphino substituents R = [5-methyl]-2-furyl = Fu, and R' = phenyl (**4a**), *i*-propyl (**4b**). A modular synthetic approach was applied from the di-*tert*-butylated ferrocene platform (**1**), which lead to the formation of new diphosphines by using 1,1'-bis(diiodo)-3,3'-bis(*tert*-butyl)ferrocene (**2**) as synthetic precursor. In contrast to the cousin non-alkylated unsymmetrically substituted diphosphino-ferrocenes which were reported up to now, these diphosphines showed strong (^{31}P, P')-nonbonded ("through-space") nuclear spin-spin coupling. The strength of such internuclear spin-spin coupling constant (SSCCs) $J_{PP'}$ ranges between 17 and 35 Hz, and as such, are not associated to traditional "through-bond" $^{4}J_{PP'}$. The characterizations of these ferrocene derivatives by X-ray diffraction in the solid state, and by multinuclear NMR in solution, evidence that the strong SSCCs are attributable to the conformational constraint which is imposed to ferrocene backbone by the introduction of alkyl substituents on this platform. The molecular structures resolved in the solid-state showed long P...P mutual separation up to 6.9168(8) Å, while in solution a (P, P')-phosphorus lone-pair overlap clearly occurs. This testifies to a sufficient degree of rotational flexibility of the alkylated ferrocene backbone. We examined the coordination chemistry of these diphosphines towards coinage metals: Cu, Ag and Au. The constraint unsymmetrically substituted diphosphines **4a** and **4b** allowed the selective formation of dinuclear two-coordinate linear gold(I) complexes with strong Au...Au aurophilic interactions. They also lead to rare tetrahedral homoleptic d^{10} monocationic complexes, with all the coinage metals, by structuring the encapsulation of the cation in a highly constraint environment where the stacking interactions of the (hetero)aromatic substituents of the phosphino groups are decisive. The resulting AA'XX' ^{31}P NMR signature in solution of the complexes was simulated and analyzed, as well as the stacking interactions between the pairs of furyl rings that were illustrated by noncovalent interactions (NCI) computation.

■ INTRODUCTION

Unequally functionalized ferrocenes are known to give access to valuable reactivity from the formation of various hemilabile species.[1] This has been especially explored for hybrid ferrocenyl phosphine ligands holding a variety of additional donor and acceptor atoms (N, S, O, Se, B, *etc.*) in diverse functional groups.[2,3] However, the synthesis of unsymmetrically substituted diphosphines of 1,1'-bis(phosphino)ferrocene structure is fairly limited (Figure 1, left).[4,5] Indeed, while heteroannular 1,1'-homofunctionalization of ferrocene is straightforward, the introduction of two different functions is more challenging, and inevitably requires optimized stepwise functionalization. Nevertheless, such unequally functionalized ferrocenyl diphosphines eventually have a specific interest in physical chemistry for further studying nuclear spin coupling properties from the direct observation in solution NMR of nonbonded ^{31}P-^{31}P' spin-spin couplings (also known as "through-space" spin-spin couplings, Figure 1, right).[6,7]

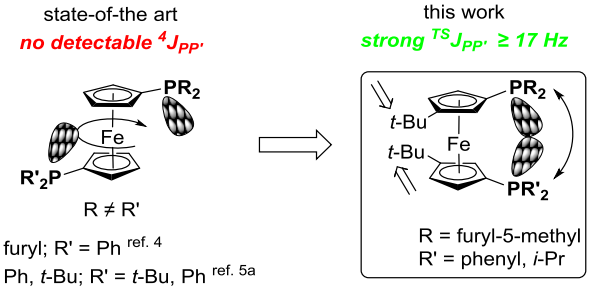

R = furyl; R' = Ph [ref. 4]
R = Ph, *t*-Bu; R' = *t*-Bu, Ph [ref. 5a]
R = Ph; R' = *i*-Pr [ref. 5b]
R = Ph, C_6H_4-4-OMe; R' = C_6H_4-4-OMe, C_6H_4-4-CF_3 [ref. 5c]
R = Ph; R' = *t*-Bu [refs. 5d,e]
R = Ph; R' = Cy, *i*-Pr, *t*-Bu [ref. 5f]

Figure 1. Unsymmetrically substituted diphosphines of 1,1'-bis(phosphino)ferrocene type (left). Noncovalent (P, P') nuclear spin

coupling (PP' SSCCs > 15 Hz) in unsymmetrically substituted alkylated bis(phosphino)ferrocenes (right).

Nuclear spin–spin couplings are among the parameters routinely used in high-resolution nuclear magnetic resonance for determining molecular structures within inorganic, organic, and biological compounds.[7] This electron-mediated coupling is characterized by the *J* spin-spin coupling constants (SSCCs), and commonly thought as being transmitted by covalently bonded atoms. However, advanced NMR studies have shown that scalar spin couplings between two proximate spin active nuclei (A, B) can commonly operate through nonbonded interactions, leading to J_{AB} coupling constants relating thus to "through-space" internuclear scalar spin–spin coupling transmission (TS couplings).[7,6b-l] Such often neglected TS spin–spin coupling process is recurrent and involved in all commonly encountered spin active nuclei for NMR studies, such as ^{1}H, ^{13}C, ^{19}F, and ^{31}P, non-exhaustively.

The application of nonbonded J_{PP} SSCCs for the structural determination in solution of organophosphorus molecules including metallocenic fragments has been developed by our group using polyphosphino ferrocenes.[8] Nonbonded $^{TS}J_{PP}$ couplings are useful for assessing the conformation of the ferrocene backbone in tri- and tetraphosphines,[8b] because the orientation of the phosphino substituents hold on the ferrocene backbone can achieve efficient P-lone-pairs overlap (Figure 1, right).[8a] When such overlap of electron lone-pairs is achieved, the spin-spin coupling of magnetically equivalent spin active nuclei exists; however, it is not directly observable on the resulting NMR spectra.[7]

Thus, a situation required for observing ^{TS}J coupling is the close spatial proximity of nonbonded chemically *nonequivalent* nuclei.[9] A separation of four covalent bonds (or more) between the nonequivalent nuclei generally nullifies any through-bond spin coupling (see state-of-the art examples in Figure 1, left). Since ferrocene backbone is an ideal platform for assembling several phosphino groups in close proximity,[10] herein we synthesized unsymmetrically substituted 1,1'-bis(phosphino)ferrocenes incorporating in addition bulky alkyl substituents for a better ferrocene backbone conformation control. Our objective was to trigger new ferrocene ligands potentially featuring strong $J_{PP'}$ SSCCs, and study their coordination chemistry properties. While several species reported by our group[4] and others[5] exist, none of them were associated to clear ^{31}P-$^{31}P'$ SSCCs (Figure 1). We now report the formation of constrained unsymmetrical bis(phosphino)ferrocenes in which the proximity of chemically *nonequivalent* phosphino groups generates strong ^{31}P-$^{31}P'$ spin coupling that are directly observable by ^{31}P NMR in solution. We studied in parallel their arrangement in the solid state by single-crystal XRD determination.

An additional interest of producing unsymmetrically functionalized 1,1'-bis(phosphino)ferrocenes is to study their role as structuring tool in transition metals coordination chemistry. For instance, notable *trans* effect on the rates of reductive elimination in aryl palladium(II) amido complexes stabilized by unsymmetrical 1,1'-bis(diphenylphosphino)ferrocenes had been reported.[5c] Using symmetrical analogues, di-*tert*-butylated-bis(phosphino)ferrocene ligands achieved the selective formation of Au^{I} halide complexes,[11] where the phosphino groups bearing (hetero)aryl or alkyl groups, exert a control on the selective formation of either dinuclear linear two-coordinate, mononuclear trigonal three-coordinate, or tetrahedral four-coordinate complexes.[11a] Given the general interest for cationic four-coordinate d^{10} gold(I) complexes for which photophysical,[12] and therapeutic properties[13] are known, we extended the studies of Au^{I} bisphosphine complexes to the general formation of unprecedented unsymmetrical cationic tetrahedral analogues in group 11.[14] The d^{10} complexes of silver(I) and copper(I) were synthesized and structurally compared to gold(I) complexes in the solid state by X-ray diffraction (XRD) and their stability was analyzed by computation of noncovalent interactions (NCI), which evidenced the crucial role of stacking interaction in the encapsulated structure of the complexes.

■ RESULTS AND DISCUSSION

Unsymmetrically substituted *tert*-butylated 1,1'-bis(phosphino) ferrocenes. We focused on the synthesis of two unsymmetrical *tert*-butylated bis(phosphino)ferrocenes holding groups which are sterically and electronically significantly differentiated, namely phenyl, *i*-propyl and [5-methyl]-2-furyl. The synthesis of substituted ferrocenyl diphosphines bearing two phosphino groups of different nature is achievable by iterative monolithiation of a 1,1'-dihaloferrocene and quenching with the appropriate halodisubstituted phosphines.[4,5c] The diastereoselectivity in the synthesis of the alkylated 1,1'-bis(diiodo)-3,3'-bis(*tert*-butyl)ferrocene **2** (Scheme 1) is attributed to the mutual steric repulsion of the bulky alkyl substituents associated with a coordination of TMEDA to lithium in the lithiated ferrocenyl dilithium precursor **1**.[15]

Scheme 1. Synthesis of *tert*-butylated bis(phosphino)ferrocenes 4a and 4b.

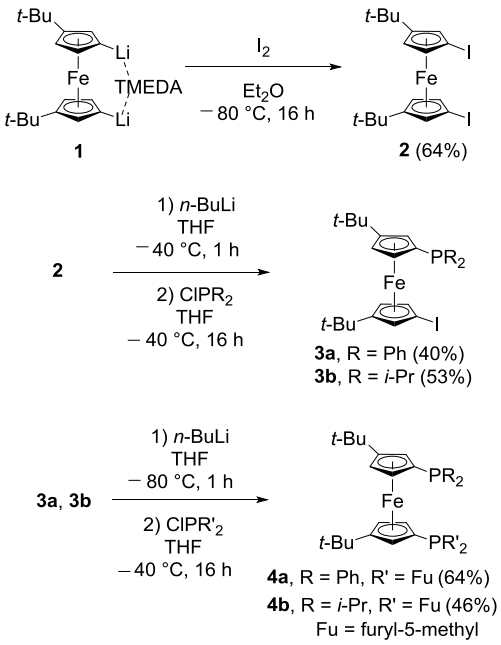

In our hands, diiodinated ferrocene **2** was easier to purify compared to its dibrominated counterpart, by using saturated $FeCl_3$ solution extraction.[3,16] The successive monolithiation and phosphination of **2** were achieved to give the monoarylphosphine **3a** and monoalkylphosphine **3b** (40% and 53% isolated yields respectively, Scheme 1).[17] Lithiation then phosphination of **3a** and **3b** gave unsymmetrical diphosphines **4a** and **4b** in 64% and 46% isolated yields, respectively (Scheme 1).

^{31}P NMR ($CDCl_3$, 298 K) for phenylphosphine **3a** and isopropylphosphine **3b** at –19.7 ppm and –1.8 ppm are consistent with the corresponding symmetrical ferrocenyl diphosphines (signals at –20.1 and –1.6 ppm, respectively).[18] The introduction of the iodine atom in 1'-position led to a stronger shift of ^{31}P signal compared to the monophosphine counterparts found at –15.0 and 0.3 ppm respectively observed as side-products. The two distinct ^{31}P NMR ($CDCl_3$, 298 K) signals of **4a** and **4b** are doublets of doublets centred at –19.1 (Ph), –65.8 (Fu) ppm, and –1.17 (*i*-Pr), –64.71 (Fu) ppm, respectively. Since the ^{31}P NMR of the previously reported unsymmetrical bis(phosphino)ferrocenes resulted in singlet signals only,[4,5c] the ^{31}(P, P') spin couplings in **4a** and **4b** are clearly attributable to "through-space" SSCCs $^{TS}J_{PP'}$ between heteroannular phosphorus, because of an adequate backbone conformation (Scheme 1) and P-lone-pair orientation for overlapping. The SSCCs values of 34.5 Hz for **4a** (Fu, Ph) and 17.1 Hz for **4b** (Fu, *i*-Pr) cannot be associated to classical $^4J_{PP}$ coupling constants that are transmitted through covalent bonding. Additionally, their magnitude nicely correlates the SSCCs found in related constraint ferrocenic polyphosphines holding three or four magnetically inequivalent nearby phosphino groups.[8a,10,19]

In solution NMR, the higher value of $^{TS}J_{PP}$ of 34.5 Hz found for **4a** compared to **4b** shows a strong influence of electronic factors from the alkyl/aryl substituents. The Fermi-contact is the dominant term to nuclear spin-spin coupling.[7,20] Fermi-contact occurs from *s* electrons and in a ^{31}(P, P') TS nuclear spin interaction withdrawing of electron density brought about by attachment of an electron-attractive substituent to a spin active nucleus (P) increases the effective nuclear charge of this atom.[20c] This charge perturbation augments the probability of the valence *s* electrons for nuclear contact. Thus, an increase of the *J* constant is expected from electron-withdrawing substituents. Considering the relative electron-transfer properties of furyl, phenyl and *i*-propyl groups, this is consistent with a stronger $^{TS}J_{PP}$ value obtained for **4a** (Fu, Ph) compared to **4b** (Fu, *i*-Pr). These spin couplings also indicate that in solution steric control is exerted by *tert*-butyl groups and contributes to a close proximity of the phosphino groups in solution, conveying an efficient nuclear spin-spin coupling by (P, P') lone-pairs overlap.

In the solid state, XRD analysis of the new compounds **3a**, **3b** and **4a**, **4b** was conducted from single crystals. The molecular structure of compounds **3a** and **3b** elucidated by XRD (crystalizing in $P2_1/c$ and P-1 space groups, respectively) showed very similar conformations with a cisoid mutual arrangement of phosphino and iodo groups (Figure 2). Torsion angles P–Ct1–Ct2–I are equal to 71.09(4) ° and 68.97(4) °, respectively. These conformations were reminiscent of the one reported for the cousin compound 1-bromo-1'-(diphenylphosphino)ferrocene,[3] featuring distances between the halogen and phosphine functions *d* P...X which ranges from 4.8723(5) Å (X = Br) to 5.0868(9) Å (X = I).

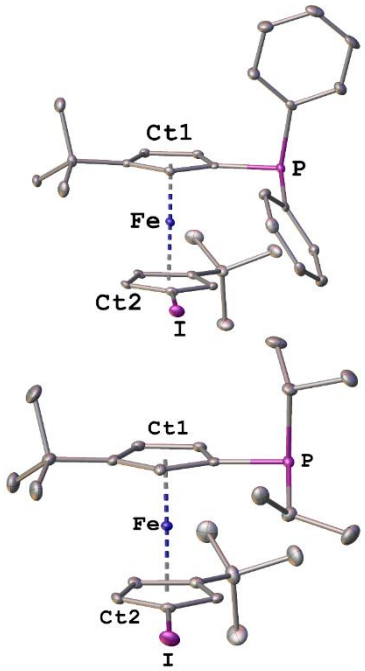

Figure 2. Molecular structures of **3a** (top), and **3b** (bottom). Hydrogen atoms are omitted for clarity. Selected bond lengths and distances (Å) and angles (deg) with Ct1 (C1-C2-C3-C4-C5) and Ct2 (C6-C7-C8-C9-C10): **3a**, Fe–Ct1 = 1.6521(13); Fe–Ct2 = 1.6526(13); C1–P = 1.812(3); C6–I = 2.088(3); *d* P...I = 5.0088(8); Ct1–Fe–Ct2 = 178.80(6); P–Ct1–Ct2–I = 71.09(4); **3b**, Fe–Ct1 = 1.656(2); Fe–Ct2 = 1.6485(17); C1–P = 1.821(4); C6–I = 2.0837(18); *d* P...I = 5.0868(9); Ct1–Fe–Ct2 = 177.80(11); P–Ct1–Ct2–I = 68.97(4).

The unsymmetrical *tert*-butylated 1,1'-bis(phosphino) ferrocenes **4a** and **4b** crystallized in $P2_1/n$ and P-1 space groups respectively (Figure 3). They presented a quasi-eclipsed conformation of their cyclopentadienyl rings. However, the very different torsion angles between the phosphino groups found in **4a** (P1–Ct1–Ct2–P2 = –49.21(5) °) and **4b** (P1–Ct1–Ct2–P2 = 156.68(3) °) induces a cisoid arrangement in **4a** where *d* P1...P2 = 3.9863(16) Å and a transoid arrangement in **4b** where *d* P1...P2 = 6.9168(8) Å (Figure 3). Investigation of the noncovalent interactions between the ferrocene substituents (Figure S3 in SI) revealed that the cisoid arrangement in **4a** is favored by CH-π interactions between the furyl and phenyl aromatic rings and one methyl of the *t*-Bu ligands. The NCI plot also revealed an interaction between the two phosphorus atoms in **4a**. Conversely, in **4b** the transoid arrangement is favored by a van der Waals interaction between the *i*-Pr groups, and two weak interactions between the lone-pair of phosphorus atoms and a C–H bond of Me groups.[21] For **4a** and **4b**, in contrast to constraint ferrocenyl tetraphosphine complexes,[8a,b] rigid difluorocyclophanes,[22] or difluoronaphthalenes,[23] the distance separating P1...P2 in the solid state is not directly correlated to *J* SSCCs value observed in solution. Indeed, in the solid state the molecular structure of **4b** showed a separation distance *d* P1...P2 = 6.9168(8) Å between –P*i*-Pr_2 and –PFu_2 groups which excludes (P, P') lone-pairs overlap. Conversely, in solution a strong TS spin-spin coupling $J_{PP'}$ = 17 Hz is unambiguously observed. This situation is due to rotational flexibility of the ferrocene platform for this ligand. A reduced steric hindrance at phosphorus atoms is provided by both *i*-propyl- and furyl- groups which thus allows a close proximity of P atoms in solution and lone pair-overlap for spin coupling.

Accordingly, these bis(diphosphino)ferrocenes are ligands for the formation of varied transition metal complexes. We report their coordination chemistry to coinage metals, Au, Cu and Ag, topical in innovative catalytic applications.[11a,18]

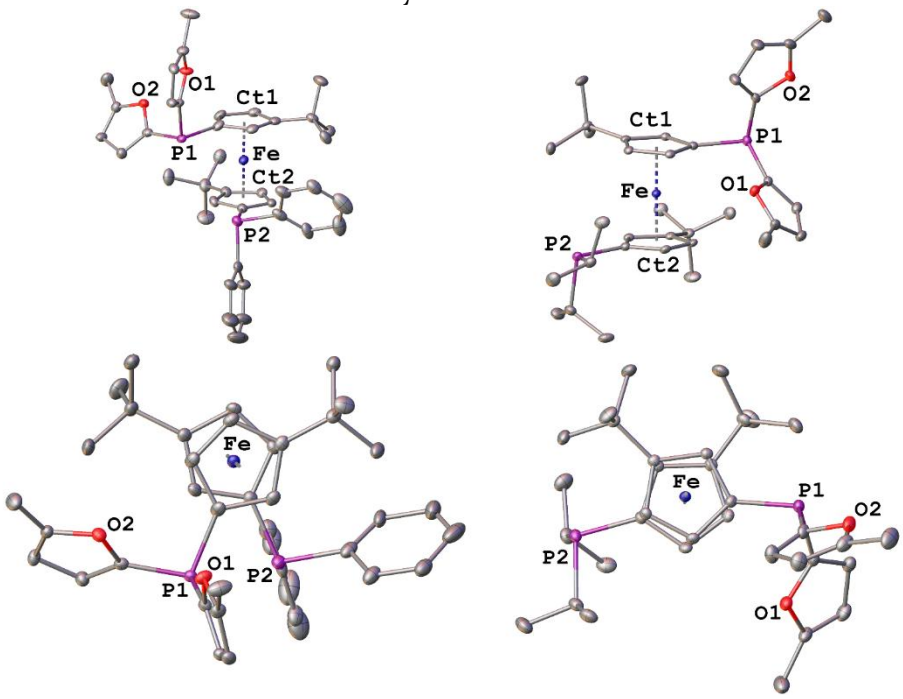

Figure 3. Molecular structures of compounds **4a** (left) and **4b** (right). Hydrogen atoms are omitted for clarity. Selected bond lengths and distances (Å) and angles (deg) with Ct1 (C1-C2-C3-C4-C5) and Ct2 (C6-C7-C8-C9-C10): **4a**: Fe–Ct1 = 1.6525(16); Fe–Ct2 = 1.6508(15); C1–P1 = 1.876(4); C6–P2 = 1.809(3); O1–O2 = 3.353(5); *d* P1...P2 = 3.9863(16); Ct1–Fe–Ct2 = 179.16(8); P1–Ct1–Ct2–P2 = –49.21(5); **4b**: Fe–Ct1 = 1.6601(9); Fe–Ct2 = 1.6630(9); C1–P1 = 1.8115(19); C6–P2 = 1.8202(19); O1–O2 = 4.236(2); *d* P1...P2 = 6.9168(8); Ct1–Fe–Ct2 = 177.48(4); P1–Ct1–Ct2–P2 = 156.68(3).

Four-coordinate mononuclear cationic group 11 complexes. We recently disclosed that the symmetrical *tert*-butylated 1,1'-bis[di(furylmethyl)phosphino]ferrocene **5** (Scheme 2, top) that is structurally related to **4a** and **4b** selectively forms the four-coordinate tetrahedral mononuclear gold(I) halide complexes [**5**-Au^+]Cl^- and [**5**-Au^+]I^- from the reaction with 0.5 equiv of gold halide salts.[11a] Their encapsulated structure identified by XRD seemed to be stabilized by stacking interactions between the four pairs of furyl rings, which exhibited centroid distances around 3.5 to 3.8 Å. We were eager to further explore such coordination chemistry with furylphosphino-based ligands by using the new dissymmetric donors **4a** and **4b**, and possibly extend it to the other coinage metals Cu and Ag.

Scheme 2. Synthesis of tetrahedral Au^I cationic complexes stabilized by two symmetrical 1,1'-bis(difurylphosphino)ferrocene ligands (top). Synthesis of the mononuclear cationic tetrahedral iodide [6-Au^+]I^- (bottom) .

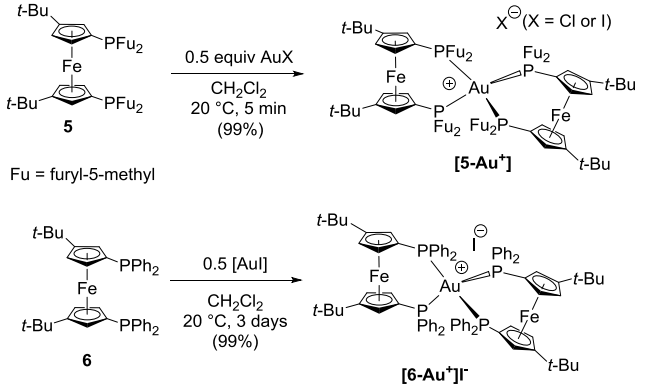

Initially, we successfully formed the mononuclear four-coordinate cationic Au^I complex [**4a-Au$^+$**]**Cl$^-$** (Scheme 3, top), albeit in notably much longer reaction times (3 days) than using the bis(difurylphosphino)ferrocene ligand **5** (5 min, Scheme 2), under unusual conditions where the halide abstraction and the formation of the cationic species was not assisted by the addition of silver salts or any noncoordinating anionic species. The same reaction conditions using the bis(di-isopropylphosphino) compound **4b** failed to selectively form mononuclear complexes, and only ill-defined mixture of species incorporating the gold(I) dinuclear complex **4b-(AuCl)$_2$** could be obtained (Scheme 3, bottom).

Scheme 3. Formation of d^{10} complexes of group 11 (Au, Ag, Cu) using 4a and 4b.

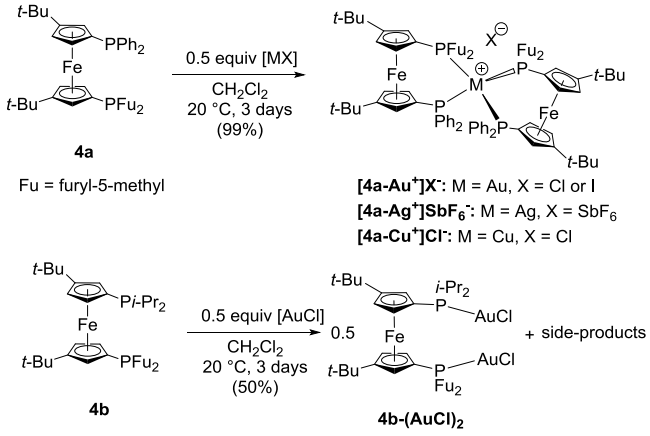

Intrigued by the difference in coordination behaviour of **4a** (bearing –PPh$_2$ groups) and **4b** (bearing –P*i*-Pr$_2$ groups) for the formation of monodentate cationic Au^I, we used the symmetrical *tert*-butylated 1,1'-bis(diphenylphosphino) ferrocene **6** in order to further stabilize a mononuclear tetrahedral homoleptic Au^I complex. Indeed, using extended reaction time conditions, we obtained the expected monodentate cationic [**6-Au$^+$**]**I$^-$** complex selectively and quantitatively (Scheme 2, bottom).

We consequently attributed the formation of these mononuclear encapsulated cationic species to an additional stability provided by inter-ligands aryl/aryl and heteroaryl/heteroaryl π stacking interactions. Our hypothesis was further supported by NCI computations (see below).

The synthesis of the analogous group 11 complexes [**4a-Ag$^+$**]**SbF$_6^-$** and [**4a-Cu$^+$**]**Cl$^-$** was further achieved selectively by reacting **4a** with 0.5 equivalent of $AgPF_6$ and CuCl, respectively (Scheme 3, top), providing the opportunity to further analyzing the tetrahedral encapsulated structures obtained with group 11 transition metals.

Solution NMR analysis of the group 11 cationic complexes. The ^{31}P NMR analysis of [**4a-Au$^+$**]**Cl$^-$**showed a typical AA'XX' spin system that was simulated at second order using G-NMR-v 5.0 (Figure 4). The analysis and simulation are consistent with two groups of magnetically inequivalent nuclei. The nuclei (A, A') correspond to –PPh2 groups resonance signals centered at 12.0 ppm, and (X, X') signals corresponding to –PFu$_2$ groups are observed at –29.5 ppm, with the corresponding set of *J* SSCCs: $J_{AA'}$ = 99 Hz, $J_{XX'}$ = 90 Hz, $J_{AX'} = J_{A'X}$ = 62 Hz and $J_{AX} = J_{A'X'}$ = 95 Hz (details in SI). The tetrahedral Au^I cationic complexes stabilized by two 1,1'-bis(diphenylphosphino)ferrocene ligands [**6-Au$^+$**]**Cl$^-$** showed in solution in ^{31}P NMR a broad signal at –12.9 ppm, while the analogous complex stabilized by two bis(difurylphosphino)ferrocene ligands [**5-Au$^+$**]**Cl$^-$** gives a resonance signal at –30.8 ppm. The complexes [**4a-Ag$^+$**]**SbF$_6^-$** and [**4a-Cu$^+$**]**Cl$^-$** displayed in ^{31}P NMR two broad signals at consistent chemical shifts, respectively: for silver, 3.7 ppm (PPh$_2$) and –39.0 ppm (PFu$_2$) and for copper, –6.0 ppm (PPh$_2$) and –40.3 ppm (PFu$_2$). VT-NMR analyses between 193 K and 300 K did not allow to achieve a better resolution of NMR spectra.

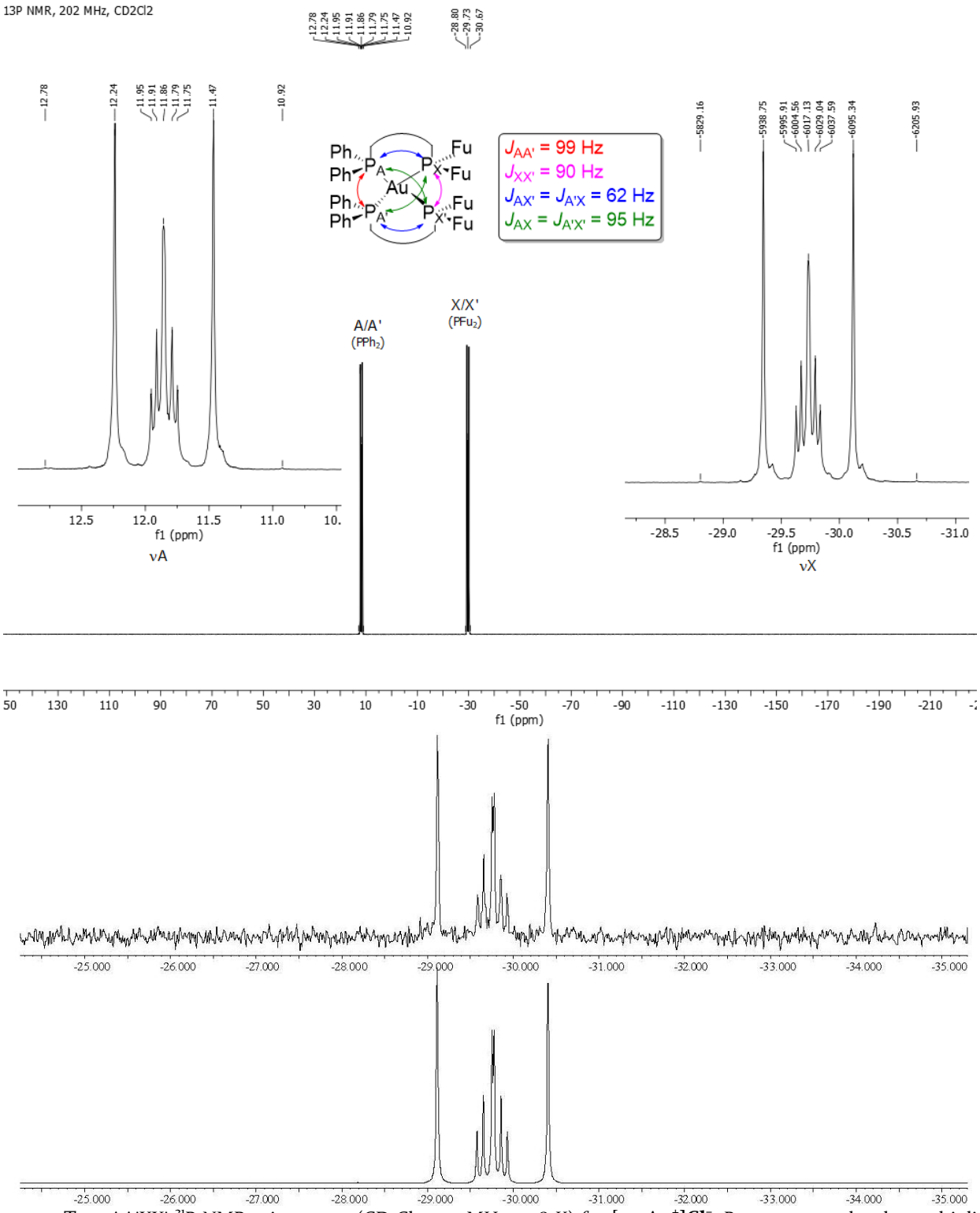

Figure 4. Top: AA'XX' ^{31}P NMR spin system (CD_2Cl_2, 202 MHz, 298 K) for [**4a-Au$^+$**]**Cl$^-$**. Bottom: second order multiplicity of furylphosphino signal with experimental and simulated spectra.

Solid state structures of [4a-Au$^+$]Cl$^-$, [4a-Ag$^+$]SbF$_6^-$, [4a-Cu$^+$]Cl$^-$ and [6-Au$^+$]I$^-$. XRD analysis were achieved from single crystals for all these complexes (Figure 5, left). For all these cationic mononuclear four-coordinate 18 ē coinage metal complexes, the M$^+$ center (M = Au, Cu, Ag) is encapsulated into a closed tetrahedral environment, globally stabilized by two hindering ferrocenyl ligands, in which the counteranion has been rejected at the periphery. In most cases, its detection from XRD analysis was difficult, when feasible. For geometry illustration, the complex [**6-Au$^+$**]**I$^-$** crystallized as a gold-centered regular tetrahedron (distances *d* Au–P1 = 2.4801(12) Å, *d* Au–P2 = 2.4761(12) Å, *d* Au–P3 = 2.4515(11) Å, *d* Au–P4 = 2.4442(12) Å and with angles equal to P1-Au-P2 = 98.28(4) °, P1-Au-P3 = 106.11(4) °; P3-Au-P4 = 103.96(4) °; P4-Au-P2 =

109.53(4) °).

The close environment arrangement benefits from the assistance of stacking interactions, originating either from furyl group or phenyl groups from the diphosphines. Consistently, the presence of *i*-Pr groups did not favored the formation of tetrahedral cationic complexes. In order to confirm this, we further analyzed the molecular structures from XRD data, using calculation and visualization of NCI between the diphosphino ferrocenyl ligands (Figure 5, right). In complexes **4a-Au**$^+$, **4a-Ag**$^+$ and **4a-Cu**$^+$, the analyses of the NCI areas confirmed the existence of strong π interactions between all four aromatic pairs (phenyl/phenyl, furyl/furyl or phenyl/furyl). This leads to a significant stabilization of the complexes that compensates the deformation energy required to form these tetrahedral complexes.[14] This is consistent with the Ag–P distances found clearly smaller than the average Ag–P distance in tetrahedral complexes [Ag^+P_4] equal to 2.6(1) Å from CCDC database compilation. A similar situation was also observed for **5-Au**$^+$. The situation is different for the complex **6-Au**$^+$ in which the NCI areas are less extended than in complexes issued of **4a** coordination. This is tentatively correlated to noncovalent stabilization that are mainly achieved from weaker CH-π interactions with only a single stronger π-π interaction (see Figure S3). As a consequence, Au–P distances are greater in **6-Au**$^+$ than in **4a-Au**$^+$. A similar arrangement of the aromatic cycles was also found in the $Ag(dppf)_2^+$ complex.[24]

Interestingly, the distribution of di-, tri-, and tetracoordination among the d^{10} ions of the group 11 metals was theoretically analyzed by means of density functional calculations on more than 150 model complexes.[14] In this study, the larger deformation energy of gold complexes compared to copper and silver ones was used to explain the predominance of dicoordination among AuI complexes, in comparison with CuI and AgI, for which dicoordination is far less common than tri- and tetracoordination. Herein, the structuring influence of the [(hetero)aryl]diphosphino ferrocene ligands is thus dominating for the final encapsulating tetrahedral coordination, whatever the nature of the coinage metal. However, the influence of π-staking interactions from second-sphere substituents (Fu, Ph) is essential in this building.

Accordingly, we further examined the influence of the unsymmetrical diphosphino-ferrocenes on the formation of topical aurophilic digold complexes, since such weak Au···Au interactions are also important for structuring gold complexes.[11]

Dinuclear gold(I) complexes and aurophilic interactions. Symmetrical *tert*-butylated 1,1'-bis(phosphino) ferrocenes have been shown very convenient ligands for forming selectively digold nuclear species.[11a] In especial, these allow avoiding the mixtures of gold species often concurrently formed in coordination with classical mono- and diphosphines, and in some cases they favored the formation of aurophilic dinuclear species otherwise elusive.[11b]

We further investigated the formation of dinuclear gold(I) halide complexes using **4a** and **4b**. We were eager to see the influence of unsymmetrical *tert*-butylated bis(phosphino) ferrocenes on the formation (or not) of Au···Au aurophilic interaction, when substituents with markedly different electron-donating and withdrawing effects are present. Does some push-pull electronic effect could be conveyed by classically weak aurophilic interactions? and how can they be identified?

In CH_2Cl_2, 2 equiv of $AuCl(SMe_2)$ (or AuI) were reacted with **4a** and **4b** to quantitatively give the corresponding complexes **4a-(AuCl)$_2$**, **4b-(AuCl)$_2$** and **4a-(AuI)$_2$** (Scheme 4, **4b-(AuI)$_2$** could not be formed). The complexes **4a-(AuCl)$_2$**, **4b-(AuCl)$_2$** and **4a-(AuI)$_2$** are characterized in ^{31}P NMR by two distinct *singlets* located, respectively, at: (*i*) 24.2 ppm (Ph) and –17.0 ppm (Fu), (*ii*) 49.2 ppm (*i*-Pr) and –16.6 ppm (Fu), (*iii*) 27.7 ppm (Ph) and –14.6 ppm (Fu). The absence of (P, P') nuclear spin-coupling is a supplementary indirect evidence of the role of lone-pairs for the TS coupling in the original ligands **4a** and **4b**, since in the formed digold complexes these lone-pairs are no longer available because of P-coordination to gold.

In the solid state, XRD analysis (Figures 6 and 7) showed that **4a-(AuCl)$_2$** effectively displays an intramolecular aurophilic interaction, $Au^1\cdots Au^2$ = 3.0393(6) Å. In **4b-(AuCl)$_2$** a significantly longer intramolecular aurophilic interaction $Au^1\cdots Au^2$ = 3.1686(4) Å was also observed. Surprisingly, for **4a-(AuI)$_2$**, in which two independent molecules are present (details in SI), significantly shorter intramolecular aurophilic interactions were also observed, with $Au^1\cdots Au^2$ = 2.9638(7) and 2.9701(7) Å. These aurophilic interactions were also visualized through NCI computations, as shown in Figure S5. This trend fully differs from the situation found within the corresponding symmetrical ferrocenyl diphosphines gold complexes, in which no aurophilic interaction between I–Au···Au–I fragments was observed.[11a] The strong Au···Au interaction formed in this case is in favor of the push-pull effect we initially anticipated from unsymmetrical diphosphines since, despite the presence of iodide, a donating effect to Au^1 could be anticipated from the $-PPh_2$ group, possibly transferred to Au^2 which undergoes electron-withdrawing from $-PFu_2$. This favoring a short Au···Au interaction for transfer. Furthermore, intermolecular interaction analyses of the XRD structures revealed a directional C–H...Cl interaction for **4a-(AuCl)2** leading to a pseudo 1D chain in the crystal. A π-π interaction was found between the furyl rings of two neighboring molecules in the **4a-(AuI)2** crystal. These non-covalent interactions are shown in SI (Figure S6 and S7).

However, as mentioned above, from solution NMR no (P, P') spin coupling between nonequivalent P atoms was observed in the complexes **4a-(AuCl)$_2$**, **4b-(AuCl)$_2$**, and **4a-(AuI)$_2$**. This indicates that if the aurophilic interactions identified in the solid state are conserved in solution –*which is not guaranteed regarding the ferrocene backbone rotational flexibility*– they do not convey nuclear spin-spin transmission between the phosphorus atoms. Curiously, the occurence of nuclear spin-spin coupling transmission through electrons involved in aurophilic bonding remains to be observed; conversely SSCCs through hydrogen bonding are known and documented.[7] An reasonable hypothesis would be that the dominant Fermi-contact contribution for nuclear spin

couplings occurs from *s* electrons with local density at nuclei, while conversely aurophilicity accounts mainly for closed-shell d^{10} electron interactions.[25] This issue remains an open question that might be further adressed in theoretical NMR investigations.

■ CONCLUSION

Constrained *tert*-butylated unsymmetrical bis(phosphino) ferrocenes in which the proximity of chemically nonequivalent phosphino groups generates strong ^{31}P-$^{31}P'$ spin coupling, which are directly observable by ^{31}P NMR in solution, are ideal tool for studying "Through-Space" nuclear spin-spin couplings. Accordingly, we reported the synthesis of new unsymmetrical di-*tert*-butylated diphosphino ferrocenes **4a** and **4b** holding $-PR_2$ and $-PR'_2$ groups, with R = [5-methyl]-2-furyl = Fu and R' = Ph and *i*-Pr. As expected, these unsymmetrical bis(phosphino) ferrocenes trigger strong ^{31}P "through-space" interaction, and by comparison with their molecular structure resolved in the solid state, display in solution a rotational flexibility controlled by their bulky alkyl groups. For the first time, some of their coordination chemistry (mononuclear) with coinage metals was examined. Homoleptic tetrahedral cationic complexes were obtained from gold, silver and copper salts. These unusual complexes are stabilized by stacking interactions between the four pairs of aromatic furyl and phenyl rings. The encapsulating structure of these complexes, spontaneously obtained in the absence of halide abstractor, was analyzed herein both by XRD and NCI calculation. The predominance of dicoordination among Au(I) complexes, in comparison with Cu(I) and Ag(I), for which dicoordination is far less common than tetracoordination, is circumvented by these original ligands. In addition, the formation of dinuclear complexes from gold exemplified for the first time Au···Au aurophilic interactions in a push-pull ligand environment.

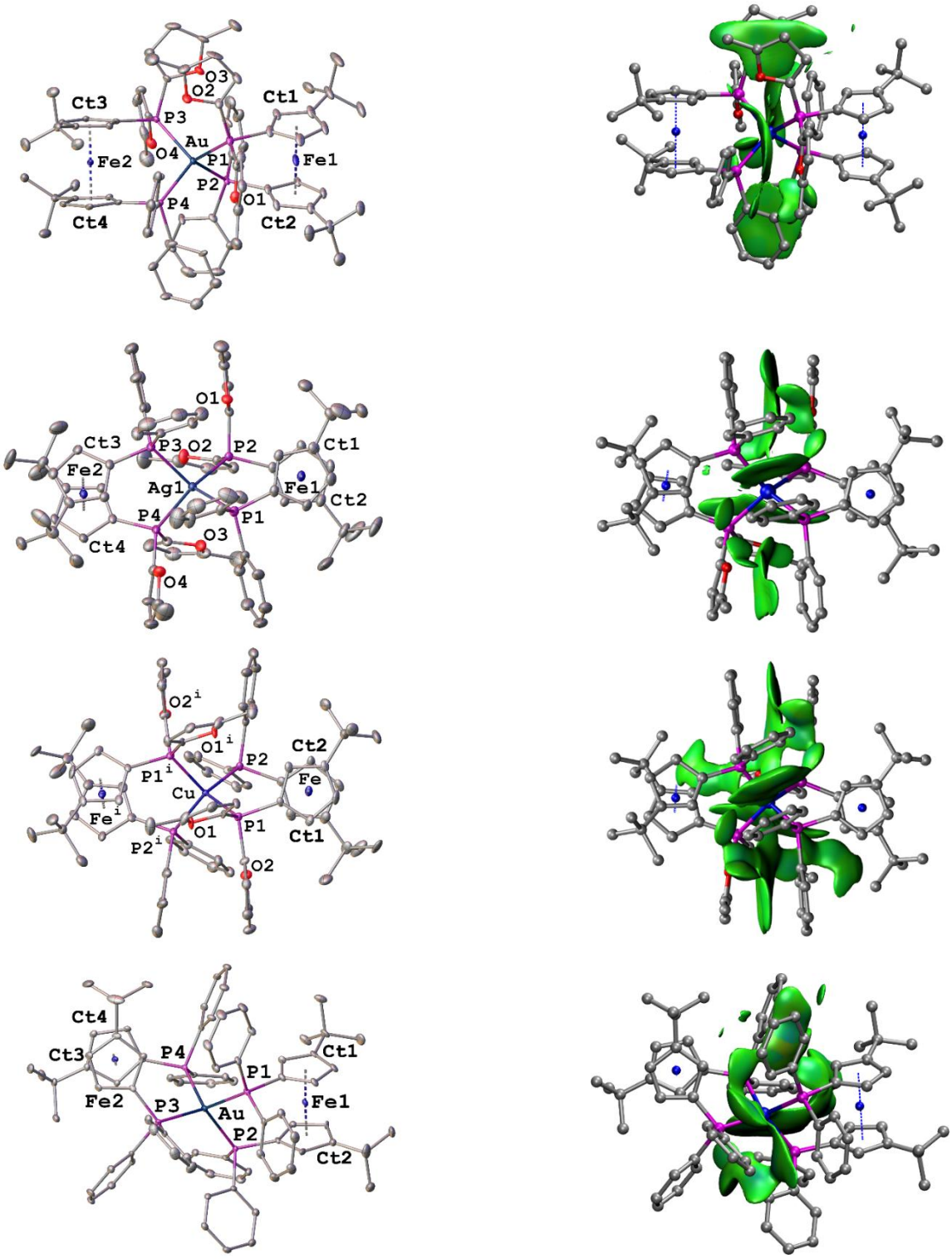

Figure 5. Molecular structures of cationic parts [**4a-Au**$^{+}$], [**4a-Ag**$^{+}$], [**4a-Cu**$^{+}$] and [**6-Au**$^{+}$] (**left**). Visualization of their corresponding NCI (right). Hydrogen atoms are omitted for clarity. Selected data for molecular structure are given in Table 1 for: [**4a-Au**$^{+}$], [**4a-Ag**$^{+}$] (two superimposable molecules are present in the asymmetric unit, only one molecule is presented in this figure, [**4a-Cu**$^{+}$] (symmetry code: (i) 1-*x*, 1-*y*, *z*), [**6a-Au**$^{+}$].

Table 1. Selected Distances (Å) and angles (deg) for [**4a-Au**$^+$], [**4a-Ag**$^+$], [**4a-Cu**$^+$] and [**6a-Au**$^+$].

param[a]	P–M (Å)		P–M–P (°)	*d* P...P (Å)		P1–Ct1–Ct2–P2 (°)	P3–Ct3–Ct4–P4 (°)	Hirshfeld volume (Å^3)
[**4a-Au**$^+$]	2.4049(11); 2.4064(11)	2.4029(11); 2.4087(11)	105.47(4); 111.26(4); 110.79(4); 112.30(4); 111.61(4); 105.53(4)	3.8289(16); 3.9683(17)	3.9828(16); 3.8307(17)	44.09(8)	42.89(6)	17.22
[**4a-Ag**$^+$]	2.5071(17); 2.5076(17)	2.5154(17); 2.5233(17)	102.77(6); 115.05(6); 114.05(5); 110.31(5); 111.14(5); 103.71(5)	3.918(2); 4.237(2)	4.150(2); 3.963(2)	43.23(9)	42.25(9)	17.67
[**4a-Cu**$^+$]	2.3296(16); 2.2953(16)		107.49(6); 111.03(6); 107.79(7)	3.730(2); 3.812(2)		40.74(9)		10.72
[**6a-Au**$^+$]	2.4801(12); 2.4761(12)	2.4515(11); 2.4442(12)	98.28(4); 106.11(4); 116.43(4); 123.22(4); 109.53(4); 103.96(4)	3.7483(18); 3.9417(16)	4.0188(18); 3.8569(15)	26.68(7)	-43.40(6)	17.99

[a] M = Au, Ag or Cu; Ct1 (C1-C2-C3-C4-C5), Ct2 (C6-C7-C8-C9-C10), Ct3 (C11-C12-C13-C14-C15) and Ct4 (C16-C17-C18-C19-C20).

Scheme 4. Dinuclear aurophilic two-coordinate gold(I) complexes synthesis from Au^I halide salt.

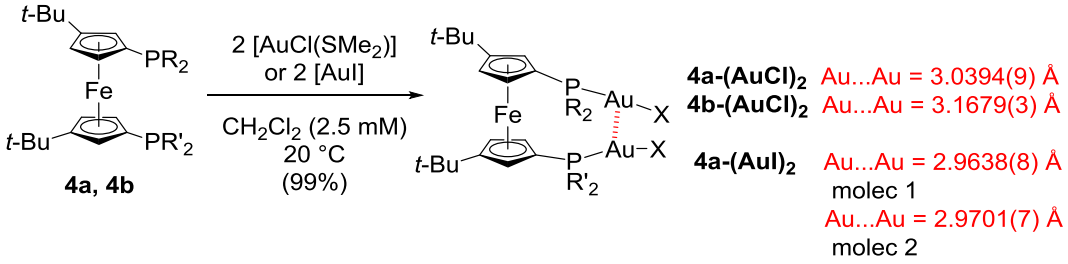

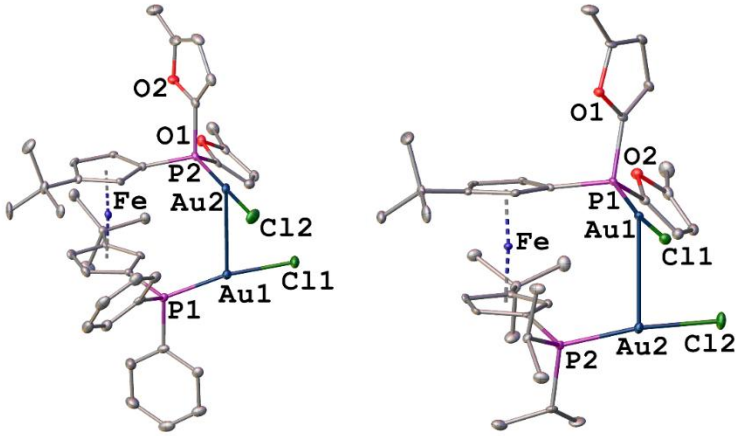

Figure 6. Molecular structures of 4a-(AuCl)2 (left), and **4b-(AuCl)2** (right). Hydrogen atoms are omitted for clarity. Selected bond lengths and distances (Å) and angles (deg): **4a-(AuCl)$_2$**: Fe–Ct1 = 1.653(3); Fe–Ct2 = 1.654(3) ; C1–P1 = 1.789(5); C6–P2 = 1.779(5); Au1–P1 = 2.2276(16); Au2–P2 = 2.2165(15); Au1–Au2 = 3.0394(9); Au1–Cl1 = 2.2974(15); Au2–Cl2 = 2.2867(16); *d* P1...P2 = 4.824(2); Ct1–Fe–Ct2 = 175.10(14); P1–Ct1–Ct2–P2 = 54.59(9); P1–Au1–Au2–P2 = –71.42(6) ; **4b-(AuCl)$_2$**: Fe–Ct1 = 1.6587(19); Fe–Ct2 = 1.6645(19); C1–P1 = 1.777(5); C6–P2 = 1.786(5); Au1–P1 = 2.2245(13); Au2–P2 = 2.2352(13); Au1–Au2 = 3.1679(3); Au1–Cl1 = 2.2978(13); Au2–Cl2 = 2.3024(13); *d* P1...P2 = 4.9266(14); Ct1–Fe–Ct2 = 173.17(9); P1–Ct1–Ct2–P2 = 52.56(6); P1–Au1–Au2–P2 = –74.19(4).

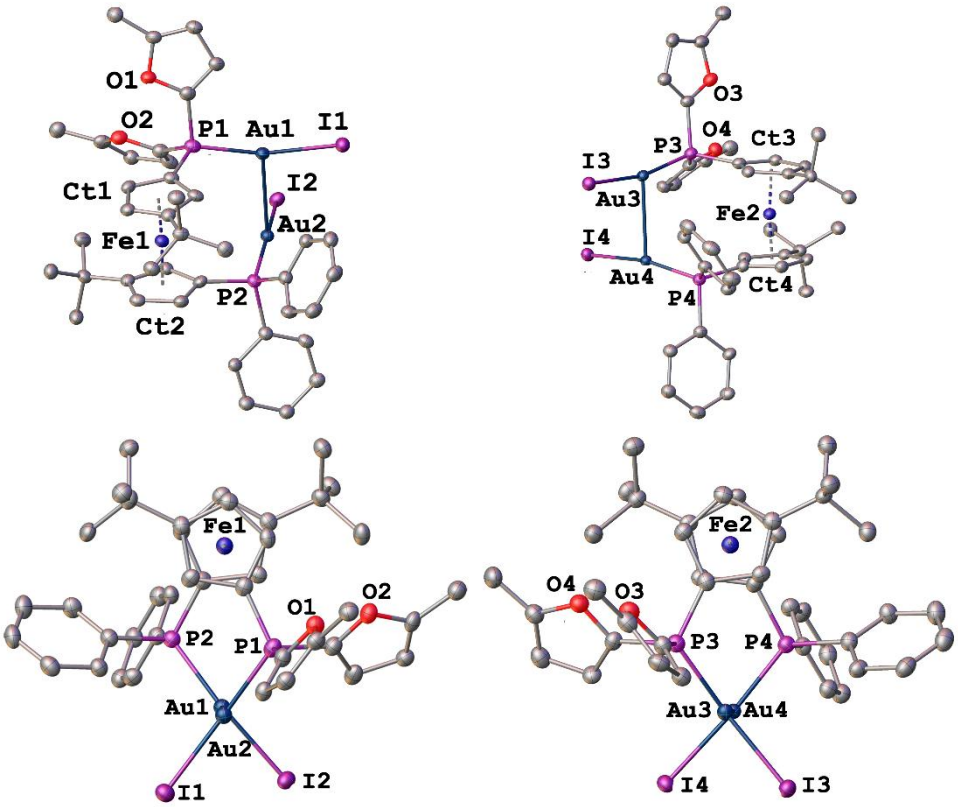

Figure 7. Views of molecular structure for **4a-(AuI)$_2$**: two independent molecules are present with side view (top) and view from above (bottom). Hydrogen atoms and one dichloromethane solvent molecule are omitted for clarity. Only the major components of the two disordered independent molecules present in the asymmetric unit are presented. Selected bond lengths and distances (Å) and angles (deg): **4a-(AuI)$_2$**: Molecule left: Fe1–Ct1 = 1.661(5); Fe1–Ct2 = 1.658(5); C1–P1 = 1.789(10); C6–P2 = 1.792(10); Au1–P1 = 2.283(3); Au2–P2 = 2.260(3); Au1–I1 = 2.5725(14); Au2–I2 = 2.5801(13); Au1-Au2= 2.9617(9); *d* P1...P2 = 4.732(4); Ct1–Fe1–Ct2 = 175.4 (2); P1–Ct1–Ct2–P2 = 55.58(15); P1–Au1–Au2–P2 = –72.00(10); Molecule right: Fe2–Ct3 = 1.655(5); Fe2–Ct4 = 1.659(4); C41–P3 = 1.804(10); C46–P4 = 1.797(10); Au3–P3 = 2.234(3); Au4–P4 = 2.259(3); Au3–I3 = 2.5729(18); Au4–I4 = 2.5790(16); Au3-Au4= 2.9699(11); *d* P3...P4 = 4.773(4); Ct3–Fe2–Ct4 = 174.8(2);P3–Ct3–Ct4–P4 = –55.55(15); P3–Au3–Au4–P4 = –72.57(10).

■ EXPERIMENTAL SECTION

General Procedures. All reagents were purchased from commercial suppliers and used without purifications. All reactions were performed under an atmosphere of dry argon in oven-dried glassware using Schlenk tubes and *vacuum*-line techniques. Solvents were dried and deoxygenated before distillation from sodium benzophenone ketyl. The identity and purity of the products were established at the "Chemical Analysis platform and Molecular Synthesis University of Burgundy" using high-resolution mass spectrometry, elemental analysis and multinuclear NMR. ^{1}H (300 or 500 MHz), ^{31}P (121.5 or 202.5 MHz), ^{13}C (75 or 125 MHz) spectra were recorded on Bruker AVANCE III instrument in $CDCl_3$ or CD_2Cl_2 solutions. Chemical shifts are reported in ppm relative to $CDCl_3$ (^{1}H: 7.26 and ^{13}C: 77.16) or CD_2Cl_2 (^{1}H: 5.32 and ^{13}C: 54.00) and coupling constants *J* are given in Hz. High resolution mass spectra (HRMS) were obtained on a Thermo LTQ-Orbitrap XL with ESI source. Flash chromatography was performed on silica gel (230-400 mesh). Elemental analysis experiments were performed Thermo Electron Flash EA 1112 Series.

Synthesis of 1,1'-bis(diiodo)-3,3'-bis(tertiobutyl)ferrocene (2)[26] To a solution of dilithium 1,1'-bis(tertiobutyl)ferrocene TMEDA salt[18] (10.5 g, 24.6 mmol) in diethyl ether (80 ml) at –80 °C is added dropwise a solution of I_2 (12.5 g, 50 mmol) in diethyl ether (200 ml). After the addition, the reaction mixture was warmed and stirred overnight at room temperature. After hydrolysis, the mixture was extracted with dichloromethane and the organic layer was removed *in vacuo*. The mixture was passed through silica gel layer with heptane. Compound **7a** was isolated in a pure form after several recrystallization in MeOH as a red crystalline solid (8.6 g, 64% yield). ^{1}H NMR ($CDCl_3$, 300 MHz): δ (ppm) = 1.25 (s, 18H, *t*-Bu), 3.87 (m, 2H, Cp), 3.94 (m, 2H, Cp), 4.37 (s, 2H, Cp).

Synthesis of 1-(diphenylphosphino)-1'-iodo-3,3'-bis(tert-butyl)ferrocene (3a) To a solution of 1,1'-bis(diiodo)-3,3'-bis(*tert*-butyl)ferrocene (6.00 g, 11.00 mmol) in THF (60.0 ml) is added dropwise a solution *n*-BuLi (6.80 ml, 11.0 mmol, 1.6 M in hexane) at –78 °C. The mixture was stirring at –78 °C during 1h30 before adding dropwise a solution of $ClPPh_2$ (2.00 ml, 11.00 mmol) in THF (10.00 ml). After the addition the reaction mixture was warmed and stirred overnight at room temperature. Then the solvent was removed in vacuo. The crude product was purified by column chromatography on silica

(toluene/heptane 40:60%), compound **3a** was isolated in a pure form as a yellow crystalline solid in hot pentane (2.63 g, 40% yield).
^{1}H NMR ($CDCl_3$, 300 MHz): δ (ppm) = 1.01 (s, 9H, *t*-Bu), 1.23 (s, 9H, *t*-Bu), 3.82 (m, 1H, Cp), 3.98 (m, 1H, Cp), 4.01 (m, 1H, Cp), 4.11 (m, 1H, Cp), 4.15 (m, 1H, Cp), 4.23 (m, 1H, Cp), 7.25–7.33 (m, 8H, Ph), 7.45-7.51 (m, 2H, Ph). ^{31}P{^{1}H} NMR ($CDCl_3$, 121 MHz): δ (ppm) = –19.7 (PPh_2). ^{13}C NMR ($CDCl_3$, 75 MHz): δ (ppm) = 30.4 [*C*(*t*-Bu)], 31.1 [*C*(*t*-Bu)], 31.5 [*C*H_3(*t*-Bu)], 31.9 [*C*H_3(*t*-Bu)], 40.6 (*Cp*^{ipso}–I), 66.7 (m, Cp), 70.1 (m, Cp), 72.2 (d, *J* = 7.3 Hz, Cp), 73.3 (d, *J* = 2.1 Hz, Cp), 75.1 (m, Cp), 76.5 (m, Cp), 76.7 (m, Cp), 77.4 (m, Cp), 103.2 (m, Cp), 106.8 [d, *J* = 4.7 Hz, *Cp*^{ipso}–C(*t*-Bu)], 128.2 (Ph), 128.3 (Ph), 128.4 (m, Ph), 128.9 (m, Ph), 133.4 (Ph) (d, *J* = 19.2 Hz, Ph), 134.7 (d, *J* = 20.6 Hz, Ph), 139.2 (d, *J* = 10.8 Hz, Ph), 140.0 (d, *J* = 11.2 Hz, Ph). Elemental analysis calcd (%) for $C_{30}H_{34}FeIP$: C, 59.23; H, 5.63; Found: C, 59.15; H, 6.00. HRMS + p ESI (m/z) $[M+H]^+$ Calcd.: 609.08705, Found: 609.08539.

Synthesis of 1-(diisopropylphosphino)-1'-iodo-3,3'-bis(tert-butyl)ferrocene (3b) To a solution of 1,1'-bis(diiodo)-3,3'-bis(*tert*-butyl)ferrocene (1.00 g, 1.82 mmol) in THF (10.00 ml) is added dropwise a solution *n*-BuLi (1.20 ml, 1.85 mmol, 1.6 M in hexane) at –40 °C. The mixture was stirring at –40 °C during 1h before adding dropwise a solution of ClP*i*-Pr_2 (0.30 ml, 1.89 mmol) in THF (5.00 ml). After the addition the reaction mixture was warmed and stirred overnight at room temperature. Then the solvent was removed in vacuum. The crude product was purified by column chromatography on silica (diethyl ether/heptane 5:95%), compound **3b** was isolated in a pure form as a red crystalline solid after recrystallization in MeOH (0.48 g, 49% yield). ^{1}H NMR ($CDCl_3$, 300 MHz): δ (ppm) = 1.03–1.17 [m, 12H, CH_3(*i*-Pr)], 1.23 (s, 9H, *t*-Bu), 1.28 (s, 9H, *t*-Bu), 1.96 [m, 1H, C*H*(*i*-Pr)], 2.09 [m, 1H, C*H*(*i*-Pr)], 3.79 (m, 1H, Cp), 3.98 (m, 2H, Cp), 4.14 (m, Cp), 4.18 (m, 1H, Cp), 4.30 (m, 1H, Cp). ^{31}P{^{1}H}($CDCl_3$, 121 MHz): δ (ppm) = –1.76 [P(*i*-$Pr)_2$]. ^{13}C NMR ($CDCl_3$, 75 MHz): δ (ppm) = 20.4 [dd, *J* = 15.0 and 11.4 Hz, CH_3(*i*-Pr)], 21.1 [dd, *J* = 15.2 and 2.3 Hz, CH_3(*i*-Pr)], 23.8 [dd, *J* = 11.9 and 4.6 Hz, *C*H(*i*-Pr)], 30.7 [*C*(*t*-Bu)], 31.1 [*C*(*t*-Bu)], 31.9 [d, *J* = 2.2 Hz, CH_3(*t*-Bu)], 32.0 [CH_3(*t*-Bu)], 42.3 (*Cp*^{ipso}–I), 66.9 (Cp), 70.0 (m, Cp), 72.3 (d, *J* = 11.2 Hz, Cp), 73.1 (m, Cp), 73.5 (d, *J* = 9.4 Hz, Cp), 74.3 (Cp), 77.4 (m), 103.8 [m, Cp*C*(*t*-Bu)], 105.2 [m, *J* = 2.0 Hz, Cp*C*(*t*-Bu)]. Elemental analysis calcd (%) for $C_{24}H_{38}FeIP$: C, 53.35; H, 7.09; Found: C, 53.23; H, 7.33. HRMS + p ESI (m/z) $[M+H]^+$ Calcd.: 541.11835, Found: 541.11635.

1-(diphenylphosphino)-1'-(di(5-methyl-2-furyl)phosphino)-3,3'-bis(tert-butyl)ferrocene (4a). To a solution of 1-(diphenylphosphino)-1'-iodo-3,3'-bis(*tert*-butyl)ferrocene (0.55 g, 0.90 mmol) in THF (5.00 ml) is added dropwise a solution *n*-BuLi (0.62 ml, 0.99 mmol, 1.6 M in hexane) at –75 °C. The mixture was stirring at –75 °C during 1h30 before adding dropwise a solution of $BrP(Fu)_2$ (0.27 g, 0.99 mmol) in THF (2.00 ml). After the addition, the reaction mixture was warmed and stirred overnight at room temperature. Then the solvent was removed in vacuo. The crude product was purified by column chromatography on silica (toluene/heptane 40:60), compound **4a** was isolated in a pure form as an orange crystalline solid (0.39 g, 64% yield). ^{1}H NMR ($CDCl_3$, 300 MHz): δ (ppm) = 0.99 (s, 9H, *t*-Bu), 1.17 (s, 9H, *t*-Bu), 2.32 (s, 3H, CH_3Fu), 2.34 (s, 3H, CH_3Fu), 3.76 (m, 1H, Cp), 4.01 (m, 1H, Cp), 4.09 (m, 1H, Cp), 4.15 (m, 1H, Cp), 4.20 (m, 1H, Cp), 4.39 (m, 1H, Cp), 5.95 (m, 1H, *H*Fu), 6.02 (m, 1H, *H*Fu), 6.37 (m, 1H, *H*Fu), 6.86 (m, 1H, *H*Fu), 7.21-7.30 (m, 5H, Ph), 7.39 (m, 3H, Ph), 7.68 (m, 2H, Ph). ^{31}P{^{1}H} NMR ($CDCl_3$, 121 MHz): δ (ppm) = –19.1 (d, *J* = 34.5 Hz, PPh_2), –65.8 [d, *J* = 34.5 Hz, $P(Fu)_2$]. ^{13}C NMR ($CDCl_3$, 75 MHz): δ (ppm) = 14.1 (*C*H_3Fu*)*, 14.1 (*C*H_3Fu*)*, 30.6 (d, *J* = 11.1 Hz, *t*-Bu), 31.6 (d, *J* = 9.0 Hz, *t*-Bu), 68.9 (Cp), 69.3 (Cp), 70.7 (d, *J* = 2.5 Hz, Cp), 72.3 (d, *J* = 2.6 Hz, Cp), 72.5 (d, *J* = 4.5 Hz, Cp), 73.1 (Cp), 73.6 (d, *J* = 8.4 Hz, Cp), 75.3 (d, *J* = 8.4 Hz, Cp), 105.1 [d, *J* = 8.3 Hz, *Cp*^{ipso}–C(*t*-Bu)], 106.0 [d, *J* = 6.7 Hz, *Cp*^{ipso}–C(*t*-Bu)], 106.8 (d, *J* = 3.8 Hz, *C*HFu), 107.1 (d, *J* = 8.1 Hz, *C*HFu), 119.5 (d, *J* = 16.1 Hz, *C*HFu), 123.1 (d, *J* = 31.2 Hz, *C*HFu), 125.4 (Ph), 127.5 (Ph), 128.1 (d, *J* = 5.6 Hz, Ph), 128.3 (d, *J* = 7.9 Hz, Ph), 128.4 (Ph), 129.2 (d, *J* = 2.6 Hz, Ph), 132.4 (d, *J* = 17.9 Hz, Ph), 135.7 (d, *J* = 20.7 Hz, Ph), 138.5 (Ph), 138.5 (d, *J* = 11.2 Hz, Ph), 141.9 (d, *J* = 12.9 Hz, Ph), 150.0 (d, *J* = 14.9 Hz, *C*Fu), 152.2 (d, *J* = 2.0 Hz, *C*Fu), 156.3 (d, *J* = 3.2 Hz, *C*Fu), 156.8 (*C*Fu). Elemental analysis calcd (%) for $C_{40}H_{44}FeO_2P_2$: C, 71.22; H, 6.57; Found: C, 70.99; H, 6.47. HRMS + p ESI (m/z) $[M+H]^+$ Calcd.: 675.22442; Found: 675.22573.

1-(diisopropylphosphino)-1'-(di(5-methyl-2-furyl)phosphino)-3,3'-bis(tert-butyl)ferrocene (4b). To a solution of 1-(di*iso*propylphosphino)-1'-iodo-3,3'-bis(*tert*-butyl)ferrocene (1.00 g, 1.82 mmol) in THF (10.00 ml) is added dropwise a solution *n*-BuLi (1.13 ml, 1.82 mmol, 1.6 M in hexane) at –40 °C. The mixture was stirring at –40 °C during 1h before adding dropwise a solution of $BrP(Fu)_2$ (0.50 g, 1.82 mmol) in THF (1.00 ml). After the addition the reaction mixture was warmed and stirred overnight at room temperature. Then the solvent was removed *in vacuum*. The crude product was purified by column chromatography on silica (diethyl ether/heptane 5:95%), compound **4b** was isolated in a pure form as an orange crystalline solid (0.45 g, 46% yield). ^{1}H NMR ($CDCl_3$, 300 MHz): δ (ppm) = 0.75–0.81 [m, 3H, CH_3(*i*-Pr)], 0.87–0.92 [m, 3H, CH_3(*i*-Pr)], 1.04–1.20 [m, 3H, CH_3(*i*-Pr)], 1.15 (s, 9H, *t*-Bu), 1.26 (s, 9H, *t*-Bu), 1.26–1.36 [m, 3H, CH(CH_3)$_2$], 1.90 [m, 1H, C*H*(*i*-Pr)], 2.04 [m, 1H, C*H*(*i*-Pr)], 2.25 (s, 3H, CH_3Fu), 2.38 (s, 3H, CH_3Fu), 3.89 (m, 2H, Cp), 3.97 (m, 1H, Cp), 4.12 (m, 1H, Cp), 4.17 (m, 1H, Cp), 4.40 (m, 1H, Cp), 5.87 (m, 2H, *H*Fu), 6.03 (m, 2H, *H*Fu), 6.28 (m, 2H, *H*Fu), 6.76 (m, 2H, *H*Fu). ^{31}P{^{1}H} NMR ($CDCl_3$, 121 MHz): δ (ppm) = –1.17 [d, *J* = 17.1 Hz, P(*i*-$Pr)_2$], –64.71 [d, *J* = 17.1 Hz, $P(Fu)_2$]. ^{13}C NMR ($CDCl_3$, 75 MHz): δ (ppm) = 14.0 (*C*H_3Fu*)*, 14.2 (*C*H_3Fu*)*, 19.2 [d, *J* = 38.2 Hz, CH_3(*i*-Pr)], 20.1 [d, *J* = 12.6 Hz, CH_3(*i*-Pr)], 20.8 [d, *J* = 15.6 Hz, CH_3(*i*-Pr)], 22.3 [d, *J* = 19.7 Hz, CH_3(*i*-Pr)], 23.3 [d, *J* = 11.3 Hz, *C*H(*i*-Pr)], 24.5 [dd, *J* = 14.1 and 2.2 Hz, *C*H(*i*-Pr)], 30.6 [*C*(*t*-Bu)], 30.9 [*C*(*t*-Bu)], 31.8 [m, *C*H_3(*t*-Bu)], 32.1 [d, *J* = 1.5 Hz, CH_3(*t*-Bu)], 68.0 [*C*H(Cp)], 69.5 [*C*H(Cp)], 70.1 [*C*H(Cp)], 70.9 [d, *J* = 18.6 Hz, *C*H(Cp)], 71.6 [d, *J* = 3.1 Hz, *C*H(Cp)], 72.2 [d, *J* = 4.8 Hz, *C*(Cp)], 73.3 [d, *J* = 36.2 Hz, *C*H(Cp)], 76.9 [m, *C*(Cp)], 104.5 [d, *J* = 4.0 Hz, *Cp*^{ipso}–(*t*-Bu)], 105.0 [d, *J* = 8.2 Hz, *Cp*^{ipso}–C(*t*-Bu)], 106.8 (d, *J* = 3.9 Hz, *C*HFu), 107.0 (d, *J* = 7.5 Hz, *C*HFu), 119.4 (d, *J* = 16.5 Hz, *C*HFu), 122.4 (dd, *J* = 27.2 and 0.7 Hz, *C*HFu), 150.4 (d,

J = 12.8 Hz, *C*Fu), 152.2 (d, *J* = 3.3 Hz, *C*Fu), 156.2 (d, *J* = 3.3 Hz, *C*Fu), 156.6 (d, *J* = 1.1 Hz, *C*Fu). Elemental analysis calcd (%) for $C_{34}H_{48}FeO_2P_2$: C, 67.33; H, 7.98; Found: C, 66.70; H, 8.37. HRMS + p ESI (m/z) $[M+H]^+$ Calcd.: 607.25572; Found: 607.25314.

General procedure for Gold, Silver and Copper complexes synthesis. A 50 ml round flask equipped with a magnetic stirring bar was charged with ferrocenyl diphosphines (1.0 eq.) and [M] (0.5 to 2.0 eq.) before addition of dichloromethane. Then the solution was stirred at room temperature during 10 min. The mixture is filtrated on Celite with dichloromethane. The solvent was then removed in vacuum to give the corresponding gold complex.

Complex [4a-Au$^+$]Cl$^-$ The complexation of **4a** (34.0 mg, 0.05 mmol) and [AuCl(SMe_2)] (7.3 mg, 0.025 mmol) affords **[4a-Au$^+$]Cl$^-$** in 99% (39.0 mg) yield as a orange crystalline solid. ^{1}H NMR (300 MHz, CD_2Cl_2): δ (ppm) = 0.84 (s, 18H, *t*-Bu), 1.09 (s, 18H, *t*-Bu), 1.50 (s, 6H, CH_3Fu), 2.16 (s, 6H, CH_3Fu), 3.68 (s, 2H, Cp), 4.15 (s, 2H), 4.29 (s, 4H, Cp), 4.94 (d, *J* = 6.75 Hz, 4H, Cp), 5.83 (d, *J* = 3.10 Hz, 2H, *H*Fu), 5.86 (d, *J* = 3.10 Hz, 2H, *H*Fu), 6.19 (d, *J* = 3.10 Hz, 2H, *H*Fu), 6.30 (d, *J* = 3.10 Hz, 2H, *H*Fu), 6.85 (m, 4H, Ph), 6.93 (t, *J* = 7.15 Hz, 4H, Ph), 7.05 (t, *J* = 7.15 Hz, 2H, Ph), 7.20 (m, 4H, Ph), 7.36 (m, 4H, Ph), 8.45 (sb, 2H, Ph). ^{31}P NMR (121 MHz, CD_2Cl_2): δ (ppm) = 11.9 (m, PPh_2), −29.8 [m, P($Fu)_2$]. AA'XX' system. Solubility troubles precluded proper ^{13}C NMR analysis. ^{13}C NMR (75 MHz, CD_2Cl_2): δ (ppm) = 13.4 (*C*H_3Fu), 14.5 (*C*H_3Fu), 31.1 [*C*(*t*-Bu)], 31.5 [*C*(*t*-Bu)], 31.7 [*C*H_3(*t*-Bu)], 70.4 (d, *J* = 26.4 Hz, Cp), 71.3 (m, Cp), 71.7 (m, Cp), 71.8 (m, Cp), 72.0 (m, Cp), 74.6 (d, *J* = 12.8 Hz, Cp), 75.6 (d, *J* = 22.4 Hz, Cp), 108.1 (C*H*Fu), 109.1 (*C*HFu), 120.2 (sb, *C*HFu), 124.2 (sb, *C*HFu), 128.4 (t, *J* = 4.7 Hz, Ph), 128.8 (Ph), 129.8 (Ph), 130.2 (Ph), 131,6 (sb, Ph), 132.0 (Ph), 132.2 (t, *J* = 7.4 Hz, Ph), 134.1 (sb, Ph), 135.6 (sb, Ph), 136.7 (sb, Ph), 144.6 (*C*Fu), 145.1 (*C*Fu), 158.0 (t, *J* = 3.0 Hz, *C*Fu), 158.2 (t, *J* = 3.0 Hz, *C*Fu). Elemental analysis calcd (%) for $C_{80}H_{88}AuClFe_2O_4P_4$: C, 60.75; H, 5.61; Found: C, 59.73; H, 5.82. HRMS + p ESI (m/z) $[M+H]^+$ Calcd.: 1545.39975; Found: m/z = 1545.39979.

Complex [4a-Ag$^+$]SbF$_6^-$ The complexation of **4a** (34.0 mg, 0.05 mmol) and [$AgSbF_6$] (8.6 mg, 0.025 mmol) affords **[4a-Ag$^+$]SbF$_6^-$** in 99% (42.0 mg) yield as a orange crystalline solid. Solubility troubles precluded proper NMR analysis. Their resolution in VT-NMR were not improved at lower temperature down to 193K. ^{1}H NMR (500 MHz, CD_2Cl_2): δ (ppm) = 0.36–0.80 (sb, 36H, *t*-Bu), 1.11 (sb, 6H, CH_3Fu), 2.29 (sb, 6H, CH_3Fu), 3.97–5.53 (sb, 12H, Cp), 6.04 (sb, 4H, *H*Fu), 6.27 (sb, 4H, *H*Fu), 6.68–7.61 (m, 20H, Ph). ^{31}P{^{1}H} NMR (202 MHz, CD_2Cl_2): δ (ppm) = 3.7 (sb, PPh_2), −39.8 [sb, P($Fu)_2$]. Solubility troubles precluded proper ^{13}C NMR analysis. Elemental analysis calcd (%) for $C_{80}H_{88}AgF_6Fe_2O_4P_4Sb$: C, 56.76; H, 5.24; Found: C, 55.48; H, 4.96. HRMS + p ESI (m/z) $[M-SbF_6]^+$: 1455.33828; Found: m/z = 1455.33443.

Complex [4a-Cu$^+$]Cl$^-$ The complexation of **4a** (34.0 mg, 0.05 mmol) and [CuCl] (2.5 mg, 0.025 mmol) affords **[4a-Cu$^+$]Cl$^-$** in 80% (28.0 mg) yield as a orange crystalline solid. ^{1}H NMR (500 MHz, CD_2Cl_2): δ (ppm) = 0.87 (s, 18H, *t*-Bu), 1.12 (s, 18H, *t*-Bu), 1.59 (s, 6H, *C*H_3Fu), 2.21 (s, 6H, *C*H_3Fu), 3.54 (s, 2H, Cp), 4.07 (s, 2H, Cp), 4.29 (d, *J* = 5.70 Hz, 4H, Cp), 4.96 (s, 4H, Cp), 5.80 (d, *J* = 3.10 Hz, 2H, *H*Fu), 5.86 (d, *J* = 3.10 Hz, 2H, *H*Fu), 6.15 (d, *J* = 3.10 Hz, 2H, *H*Fu), 6.17 (d, *J* = 3.10 Hz, 2H, *H*Fu), 6.62 (sb, 2H, Ph), 6.84 (t, *J* = 7.00 Hz, 2H, Ph), 6.95 (t, *J* = 7.00 Hz, 4H, Ph), 7.08 (t, *J* = 7.00 Hz, 2H, Ph) 7.20 (m, 4H, Ph), 7.35 (sb, 4H, Ph), 8.49 (q, *J* = 7.00 Hz, 2H, Ph). Solubility troubles precluded proper ^{31}P NMR analysis. ^{31}P{^{1}H} NMR (202 MHz, CD_2Cl_2): δ (ppm) = −3.7 (sb, PPh_2), −39.6 [sb, P($Fu)_2$]. ^{13}C NMR (125 MHz, CD_2Cl_2): δ (ppm) = 13.5 (*C*H_3Fu), 14.5 (*C*H_3Fu), 31.1 [*C*(*t*-Bu)], 31.6 [*C*H_3(*t*-Bu)], 31.8 [*C*H_3(*t*-Bu)], 68.6 (t, *J* = 24.9 Hz, Cp), 70.3 (Cp), 70.6 (Cp), 71.1 (t, *J* = 11.2 Hz, Cp), 71.4 (t, *J* = 10.1 Hz, Cp), 73.4 (t, *J* = 18.1 Hz, Cp), 74.4 (Cp), 74.6 (Cp), 108.2 *C*HFu), 109.0 (*C*HFu), 109.5 (q, *J* = 3.2 Hz, *C*HFu), 120.7 (*C*HFu), 124.6 (*C*HFu), 128.4 (sb, Ph), 128.6 (sb, Ph), 128.8 (t, *J* = 7.2 Hz, Ph), 129.7 (Ph), 130.0 (Ph), 132.2 (Ph), 132.4 (sb, Ph), 134.3 (Ph), 135.0 (t, *J* = 16.5 Hz, Ph), 135.7 (t, *J* = 13.4 Hz, Ph), 144.9 (t, *J* = 31.6 Hz, *C*Fu), 147.0 (t, *J* = 30.1 Hz, *C*Fu), 157.9 (t, *J* = 2.6 Hz, *C*Fu), 158.2 (t, *J* = 2.9 Hz, *C*Fu). Elemental analysis calcd (%) for $C_{80}H_{88}ClCuFe_2O_4P_4$: C, 66.35; H, 6.13; Found: C, 65.88; H, 6.47. HRMS + p ESI (m/z) $[M-Cl]^+$ Calcd: 1411.362789; Found: m/z = 1411.36157.

Complex [6-Au$^+$]I$^-$ The complexation of **6** (33.3 mg, 0.05 mmol) and AuI (8.1 mg, 0.025 mmol) affords **[6-Au$^+$]I$^-$** in 99% (41.0 mg) yield after precipitation in CH_2Cl_2 by addition of pentane as a orange crystalline solid. ^{1}H NMR (500 MHz, CD_2Cl_2): δ (ppm) = 0.93 (s, 36H, *t*-Bu), 3.83 (s, 4H, Cp), 4.23–4.29 (m, 8H, Cp), 7.02–7.44 (m, 40H, Ph). ^{31}P{^{1}H} NMR (202 MHz, CD_2Cl_2): δ (ppm) = 12.9 (s, PPh_2). Solubility troubles precluded proper ^{13}C NMR analysis. ^{13}C NMR (125 MHz, CD_2Cl_2): δ (ppm) = 31.0 [*C*(*t*-Bu)], 31.5 [*C*H_3(*t*-Bu)], 70.0 [sb, *C*H(Cp)], 72.7 [sb, *C*H(Cp)], 74.4 [sb, *C*H(Cp)], 76.4 (sb, *C*Cp), 108.0 [sb, *Cp^{ipso}*–C(*t*-Bu)], 120.1 (sb, Ph), 128.9 (sb, Ph), 130.7 (sb, Ph), 131.3 (sb, Ph), 133.5 (sb, Ph), 135.3 (sb, Ph), 137.6 (sb, Ph). Elemental analysis: Calcd (%) for $C_{84}H_{88}AuFe_2IP_4 \cdot 1.7CH_2Cl_2$: C 57.14, H 5.11. Found: C 57.06 H 5.09. HRMS + p ESI (m/z) $[M-I]^+$ Calcd.: 1529.42009; Found: 1529.42445.

Complex 4a-(AuCl)$_2$ The complexation of **4a** (34.0 mg, 0.05 mmol) and [AuCl(SMe_2)] (29.0 mg, 0.10 mmol) affords **4a-(AuCl)$_2$** in 99% (57.0 mg) yield as a orange crystalline solid. ^{1}H NMR (300 MHz, CD_2Cl_2): δ (ppm) = 0.77 (sb, 9H, *t*-Bu), 1.11 (s, 9H, *t*-Bu), 2.30 (s, 3H, CH_3Fu), 2.39 (s, 3H, CH_3Fu), 4.16 (s, 1H, Cp), 4.45 (s, 3H, Cp), 4.54 (s, 1H, Cp), 4.79 (sb, 1H, Cp), 6.03 (s, 1H, *H*Fu), 6.21 (s, 1H, *H*Fu), 6.57 (sb, 1H, *H*Fu), 7.19 (sb, 1H, *H*Fu), 7.35–7.41 (m, 4H, Ph), 7.54–7.56 (m, 4H, Ph), 8.19 (sb, 2H, Ph). ^{31}P{^{1}H} NMR (121 MHz, CD_2Cl_2): δ (ppm) = 26.1 (sb, PPh_2), −15.0 [sb, P($Fu)_2$]. Solubility troubles precluded proper ^{13}C NMR analysis. ^{13}C NMR (75 MHz, CD_2Cl_2): δ (ppm) = 14.3 (*C*H_3Fu), 14.6 (*C*H_3Fu), 30.8 [*C*(*t*-Bu)], 31.1 [*C*H_3(*t*-Bu)], 71.0 (sb, Cp), 72.9 (sb, Cp), 73.6 (sb, Cp), 74.0 (sb, Cp), 108.1 [sb, *C*HFu], 109.1 sb, *C*HFu], 128.9 (sb, Ph), 129.3 (Ph), 129.5 (Ph), 133.0 (sb, Ph), 135.6 (Ph), 160.9 (*C*Fu), 161.2 (*C*Fu). Elemental analysis: calcd (%) for $C_{40}H_{44}Au_2Cl_2FeO_2P_2$: C 42.17, H 3.89; Found: C 42.08, H 3.90. HRMS + p ESI (m/z) $[M-Cl]^+$ Calcd.: 1103.11857; Found: 1103.11980.

Complex 4b-(AuCl)$_2$ The complexation of **4b** (30.0 mg,

0.05 mmol) and [AuCl(SMe$_2$)] (29.0 mg, 0.10 mmol) affords **4b-(AuCl)$_2$** in 99% (66.0 mg) yield as a orange crystalline solid. ^{1}H NMR (300 MHz, CD_2Cl_2): δ (ppm) = 1.07 (s, 9H, *t*-Bu), 1.14 [dd, *J* = 18.27 and 6.91 Hz, 3H, C*H*$_3$(*i*-Pr)], 1.43 [dd, *J* = 16.15 and 6.87 Hz, 3H, C*H*$_3$(i-Pr)], 1.29 (s, 9H, *t*-Bu), 1.75–1.60 [m, 3H, C*H*$_3$(*i*-Pr)], 2.16 [q, *J* = 7.24 Hz, C*H*(*i*-Pr)], 2.30 (s, 3H, C*H*$_3$Fu), 2.41 (s, 3H, C*H*$_3$Fu), 2.68 [sb, 1H, C*H*(*i*-Pr)], 4.22 (s, 1H, Cp), 4.28 (d, *J* = 4.19 Hz, 1H, Cp), 4.46 (s, 1H, Cp), 4.59 (s, 1H, Cp), 4.65 (d, *J* = 4.19 Hz, 1H, Cp), 4.79 (sb, 1H, Cp), 6.03 (s, 1H, *H*Fu), 6.24 (s, 1H, *H*Fu), 6.57 (sb, 1H, *H*Fu), 7.92 (sb, 1 H, *H*Fu). ^{31}P{^{1}H} NMR (121 MHz, CD_2Cl_2): δ (ppm) = 49.2 [s, P(*i*-Pr)$_2$], –16.7 [s, P(Fu)$_2$]. Solubility troubles precluded proper ^{13}C NMR analysis. ^{13}C NMR (75 MHz, CD_2Cl_2): δ (ppm) = 14.2 (*C*H$_3$Fu), 14.5 (*C*H$_3$Fu), 19.3 [*C*H$_3$(*i*-Pr)], 19.7 [*C*H$_3$(*i*-Pr)], 20.8 [sb, *C*H$_3$(*i*-Pr)], 22.7 [sb, C*H*(*i*-Pr)], 27.4 [*C*H(*i*-Pr)], 27.9 [CH(*i*-Pr)], 30.9 [*C*(*t*-Bu)], 31.3 [*C*(*t*-Bu)], 31.4 [sb, *C*H$_3$(*t*-Bu)], 32.0 [sb, *C*H$_3$(*t*-Bu)], 70.5 (sb, Cp), 71.6 (sb, Cp), 73.8 (d, *J* = 6.2 Hz, Cp), 108.1, [d, *J* = 7.6 Hz, *C*HFu), 108.8 [d, *J* = 9.6 Hz, *C*HFu), 160.7 (d, *J* = 5.3 Hz, *C*Fu). Elemental analysis calcd (%) for $C_{34}H_{48}Au_2Cl_2FeO_2P_2$: C, 38.12; H, 4.52; Found: C, 37.19; H, 4.42. HRMS + p ESI (m/z) [M-Cl]$^+$ Calcd.: 1035.14987; Found: 1035.14979.

Complex 4a-(AuI)$_2$ The complexation of **4a** (34.0 mg, 0.05 mmol) and [AuI] (32.0 mg, 0.10 mmol) affords **4a-(AuI)$_2$** in 99% (66.0 mg) yield as a orange crystalline solid. ^{1}H NMR (300 MHz, CD_2Cl_2): δ (ppm) = 0.88 (sb, 9H, *t*-Bu), 1.10 (s, 9H, *t*-Bu), 2.31 (s, 3H, C*H*$_3$Fu), 2.40 (s, 3H, C*H*$_3$Fu), 4.16 (s, 1H, Cp), 4.50–4.61 (m, 5H, Cp), 6.06 (s, 1H, *H*Fu), 6.18 (s, 1H, *H*Fu), 6.68 (sb, 1H, *H*Fu), 7.31–7.41 (m, 4H, Ph), 7.49–7.58 (m, 3H, Ph), 7.77 (sb, 1H, Ph), 8.11 (sb, 2H, Ph). ^{31}P{^{1}H} NMR (121 MHz, CD_2Cl_2): δ (ppm) = 29.6 (s, PPh_2), –12.0 [s, P(Fu)$_2$]. Solubility troubles precluded proper ^{13}C NMR analysis. ^{13}C NMR (75 MHz, CD_2Cl_2): δ (ppm) = 14.4 (*C*H$_3$Fu), 14.7 (*C*H$_3$Fu), 30.9 [*C*(*t*-Bu)], 31.1 [*C*H$_3$(*t*-Bu)], 70.4 (sb, Cp), 73.0 (Cp), 73.4 (sb, Cp), 108.1 (d, *J* = 8.8 Hz, *C*HFu), 108.6 (d, *J* = 9.5 Hz, *C*HFu), 129.4 (d, *J* = 11.6 Hz, Ph), 129.8 (d, *J* = 12.0 Hz, Ph), 131.5 (sb, Ph), 132.6 (Ph), 132.9 (sb, Ph), 135.9 (sb, Ph), 160.2 (*C*Fu), 160.8 (d, *J* = 4.7 Hz, *C*Fu). HRMS + p ESI (m/z) [M-I]$^+$ Calcd.: 1195.05419; Found: 1195.05325.

Computational details. Quantum mechanics calculations were performed with the Gaussian16 software package.[27] Energies were computed by density functional theory with the global hybrid B3PW91 exchange-correlation functional,[28] with def2-SVP basis set using experimental X-Ray geometries. Dispersion effects were taken into account using the empirical correction proposed by Grimme with a Becke-Johnson damping, denoted by D3 in the following.[29] Non Covalent Interactions were computed and visualized using IGMPLOT.[30] All NCI surfaces were plotted with an isovalue of 0.006 a.u. The Hirshfeld surfaces were computed and plotted using CrystalExplorer21.[31]

■ ASSOCIATED CONTENT

Supporting Information.

The supporting Information is available free of charge on the ACS Publications website at DOI:---

Experimental procedures and spectral data for all new compounds, NCI of **6-Au**, Hirshfeld surfaces (PDF).

Crystallographic data (CIF). CCDC 1405170 (**3a**), 1405171 (**3b**), 1405174 (**4a**), 1405175 (**4b**), 2089399 ([**4a-Au$^+$**]**Cl$^-$**), 2089400 ([**4a-Ag$^+$**]**SbF$_6^-$**), 2089401 ([**4a-Cu$^+$**]**Cl$^-$**), 2089402 ([**4a-Au$^+$**]**I$^-$**), 2089403 (**4a-(AuCl)$_2$**), 2089404 (**4b-(AuCl)$_2$**), 2089405 (**4a-(AuI)$_2$**) contain the supplementary crystallographic data for this paper. These data can be obtained free of charge from The Cambridge Crystallographic Data Centre.

■ AUTHOR INFORMATION

Corresponding Authors

*E-mail: julien.roger@u-bourgogne.fr

*E-mail: jean-cyrille.hierso@u-bourgogne.fr

ORCID

Helene Cattey: 0000-0002-4416-7510

Nadine Pirio: 0000-0003-4921-2912

Paul Fleurat-Lessard: 0000-0003-3114-2522

Jean-Cyrille Hierso: 0000-0002-2048-647X

Julien Roger: 0000-0002-4964-366X

Notes

The authors declare no competing financial interest.

■ ACKNOWLEDGMENTS

Calculations were performed using HPC resources from DNUM CCUB (Centre de Calcul de l'Université de Bourgogne). This work was supported by the ANR-PRC 2016 program (ALCATRAS, ANR-16-CE07-0001-01), the CNRS, the Université de Bourgogne, the Conseil Régional Bourgogne Franche-Comté (CHIMENE project, PhD grant for T.-A. N.) and the PIA-excellence ISITE-BFC program (COMICS project: Chemistry of Molecular Interactions Catalysis and Sensors) and the Fonds Européen de Développement Régional (FEDER).

TOC Graphic

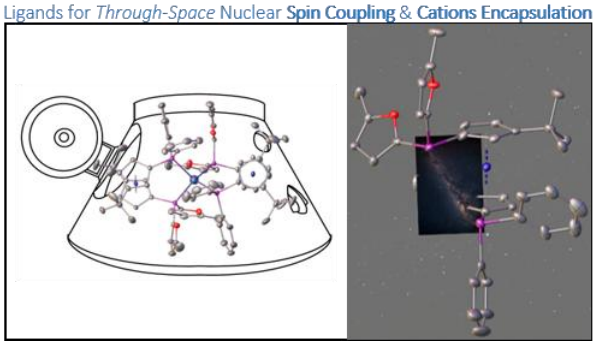

■ REFERENCES

[1] (a) Atkinson, R. C. J.; Gibson, V. C.; Long, N. J. The syntheses and catalytic applications of unsymmetrical ferroceneligands. *Chem. Soc. Rev.* **2004**, *33*, 313–328; (b) Dwadnia, N.; Roger, J.; Pirio, N.; Cattey, H.; Hierso, J. C. Input of P, N-(phosphanyl, amino)-ferrocene hybrid derivatives in late transition metals catalysis. *Coord. Chem. Rev.* **2018**, *355*, 74–100.

[2] (a) Gan, K.-S.; Hor, T. S. A. 1,1'-Bis(diphenylphosphino)ferrocene — Coordination Chemistry, Organic Syntheses, and Catalysis. In *Ferrocenes: Homogeneous Catalysis, Organic Synthesis Materials Science*; Togni, A., Hayashi, T., Eds.; Wiley-VCH: Weinheim, 1995; ch. 1, pp 3–104; (b) Štěpnicka, P., Ed., *Ferrocenes: Ligands, Materials and Biomolecules*; Wiley: Chichester, 2008; (c) Dai, L.-X.; Hou, X.-L. Eds., *Chiral Ferrocenes in Asymmetric Catalysis: Synthesis and Applications*; Wiley-VCH: Weinheim, 2010; (a) Atkinson, R. C. J.; Gibson, V. C.; Long, N. J. The syntheses and catalytic applications of unsymmetrical ferrocene ligands. *Chem. Soc. Rev.* **2004**, *33*, 313–328; (b) Guiry, P. J.; Saunders, C. P. The development of bidentate P,N ligands for asymmetric catalysis. *Adv. Synth. Catal.* **2004**, *346*, 497–537; (c) McManus, H. A.; Guiry, P. J. Recent developments in the application of oxazoline-containing ligands in asymmetric catalysis. *Chem. Rev.* **2004**, *104*, 4151–4202; (d) Arrayás, R. G.; Adrio, J.; Carretero, J. C. Recent applications of chiral ferrocene ligands in asymmetric catalysis. *Angew. Chem. Int. Ed.* **2006**, *45*, 7674–7715; (e) Miyakea, Y.; Nishibayashi, Y.; Uemura, S. Diastereoselective allylation of a chiral imine with allylzinc reagents: diastereoselective synthesis of a novel broad spectrum carbapenem. *Synlett* **2008**, *12*, 1747–1758; (f) Lu, Z.; Ma, S. Metal-catalyzed enantioselective allylation in asymmetric synthesis. *Angew. Chem. Int. Ed.* **2008**, *47*, 258–297; (g) Hargaden, G. C.; Guiry, P. J. Recent applications of oxazoline-containing ligands in asymmetric catalysis. *Chem. Rev.* **2009**, *109*, 2505–2550; (h) Malacea, R.; Poli, R.; Manoury, E. Asymmetric hydrosilylation, transfert hydrogenation and hydrogenation of ketones catalyzed by iridium complexes. *Coord. Chem. Rev.* **2010**, *254*, 729–752; (i) Zhanga, W. H.; Chiena, S. W.; Hor, T. S. A. Recent advances in metal catalysts with hybrid ligands. *Coord. Chem. Rev.* **2011**, *255*, 1991–2024; (j) Schaarschmidt, D.; Lang, H. Selective syntheses of planar-chiral ferrocenes. *Organometallics* **2013**, *32*, 5668–5704; (k) Toma, S.; Csizmadiová, J.; Meciarová, M.; Šebesta, R. Ferrocene phosphane-heteroatom/carbon bidentate ligands in asymmetric catalysis. *Dalton Trans.* **2014**, *43*, 16557–16579; (h) Radal, L.; Vosáhlo, P.; Roger, J.; Cattey, H.; Amardeil, R.; Císařová, I.; Štěpnička, P.; Pirio, N.; Hierso, J.-C. Highly Functionalized Brønsted Acidic/Lewis Basic Hybrid Ferrocene Ligands: Synthesis and Coordination Chemistry. *Eur. J. Inorg. Chem.* **2019**, *2019*, 865–874; (i) Lerayer, E.; Radal, L.; Nguyen, T. A.; Dwadnia, N.; Cattey, H.; Amardeil, R.; Pirio, N.; Roger, J.; Hierso, J.-C. Highly Functionalized Ferrocenes. *Eur. J. Inorg. Chem.* **2020**, *2020*, 419–445.

[3] Lerayer, E.; Renaut, P.; Roger, J.; Pirio, N.; Cattey, H.; Devillers, C. H.; Lucas, D.; Hierso, J.-C. A general diastereoselective synthesis of highly functionalized ferrocenyl ambiphiles enabled on a large scale by electrochemical purification. *Chem. Commun.* **2017**, *53*, 6017−6020.

[4] Fihri, A.; Hierso, J.-C.; Vion, A.; Nguyen, D. H.; Urrutigoïty, M.; Kalck, P.; Amardeil, R.; Meunier, P. Diphosphines of dppf- Type Incorporating Electron- Withdrawing Furyl Moieties Substantially Improve the Palladium- Catalysed Amination of Allyl Acetates. *Adv. Synth. Catal.* **2005**, *347*, 1198–1202.

[5] (a) Butler, I. R.; Cullen,Kim, T.-J. Synthesis of some (isopropyl)phosphinoferrocenes. *Synth. React. Inorg. Met.-Org. Chem.* **1985**, *15*, 109–116; (b) Butler, I. R.; Cullen, W. R., Kim, T.-J., Rettig, S. J.; Trotter, J. 1,1'-Bis[(alkyl/aryl)phosphino]ferrocenes: Synthesis and Metal Complex Formation. Crystal Structure of Three Metal Complexes of $Fe(\eta^5\text{-}C_5H_4PPh_2)_2$. *Organometallics* **1985**, *4*, 972–980; (c) Yamashita, M.; Cuevas Vicario, J. V.; Hartwig, J. F. Trans Influence on the Rate of Reductive Elimination. Reductive Elimination of Amines from Isomeric Arylpalladium Amides with Unsymmetrical Coordination Spheres. *J. Am. Chem. Soc.* **2003**, *125*, 16347–16360; (d) Kahn, S. L.; Breheney, M. K.; Martnak, S. L.; Fosbenner, S. M.; Seibert, A. R.; Kassel, W. S.; Dougherty, Nataro, C. Synthesis, Characterization, and Electrochemistry of Compounds Containing 1-Diphenylphosphino-1'-(di-tert-butylphosphino)ferrocene (dppdtbpf). *Organometallics* **2009**, *28*, 2119–2126; (e) Hartlaub, S. F.; Lauricella, N. K., Ryczek, C., N.; Furneaux, A. G.; Melton, J. D.; Piro, N. A.; Kassel, W. S.; Nataro, C. Late Transition Metal Compounds with 1,1'-Bis(phosphino)ferrocene Ligands. *Eur. J. Inorg. Chem.* **2017**, *2017*, 424–432; (f) Vosahlo, P.; Cisarova, I.; Stepnicka, P. Comparing the asymmetric dppf-type ligands with their semi-homologous counterparts. *J. Organomet. Chem.* **2018**, *860*, 14–29.

[6] (a) Harris, R. K.; Grinter, R. Nuclear spin-spin coupling. In *Nuclear Magnetic Resonance: vol. 2*, Harris, R. K. Ed.; The Chemical Society, Burlington House: London, 1972: pp 50–111; (b) Hilton, J.; Sutcliffe, L. H. The "through-space" mechanism in spin spin coupling. *Prog. Nucl. Magn. Reson. Spectrosc.* **1975**, *10*, 27–39; (c) Contreras, R. H.; Natiello, M. A.; Scuseria, G. E. Mechanisms which produce spin-spin coupling in NMR. *Magn. Reson. Rev.* **1985**, *9*, 239–321; (d) Contreras, R. H.; Facelli, J. C. Advances in Theoretical and Physical Aspects of Spin-Spin Coupling Constants. *Ann. Rep. NMR Spectrosc.* **1993**, *27*, 255–356; (e) Contreras, R. H.; Peralta, J. E. Angular dependence of spin-spin coupling constants. *Progr. Nucl. Magn. Reson.* **2000**, *37*, 321–425; (f) Contreras, R. H.; Peralta, J. E.; Giribet, C. G.; Ruiz de Azúa, M. C.; Facelli, J. C. Advances in Theoretical and Physical Aspects of Spin-Spin Coupling Constants. *Ann. Rep. NMR Spectrosc.* **2000**, *41*, 55–184; (g) Webb, G. A.; Fukui, H.; Baba, T. Theoretical aspects of spin-spin couplings. In *Nuclear Magnetic Resonance: vol. 32*, Webb, G. A. Ed.; The Royal Society of Chemistry, Thomas Graham House: Cambridge, 2003, pp 126–145; (h) Contreras, R. H.; Barone, V.; Facelli, J. C.; Peralta, J. E. Advances in Theoretical and Physical Aspects of Spin-Spin Coupling Constants. *Ann. Rep. NMR Spectrosc.* **2003**, *51*, 167–260; (i) Malkina, O. L. Interpretation of Indirect Nuclear Spin-Spin Coupling Constants. In *Calculation of NMR and EPR Parameters*, Kaupp, M.; Bühl, M.; Malkin, V., Eds.; Wiley-VCH: Weinheim, 2004, pp 307–324; (j) Krivdin, L. B.; Contreras, R. H. Recent Advances in Theoretical Calculations of Indirect Spin-Spin Coupling Constants. *Ann. Rep. NMR Spectrosc.* **2007**, *61*, 133–245; (k) Alkorta, I.; Elguero, J.; Denisov, G. S. A review with comprehensive data on experimental indirect scalar NMR spin-spin coupling constants across hydrogen bonds. *Magn. Reson. Chem.* **2008**, *46*, 599–654; (l) Chalmers, B. A.; Nejman, P. S.; Llewellyn, A. V.; Felaar, A. M.; Griffiths, B. L.; Portman, E. I.; Gordon, E.-J. L.; Fan, K. J. H.; Woolins, J. D., Bühl, M.; Malkina, O. L.; Cordes, D. B.; Slawin, A. M. Z.; Kilian. P. A study of through-space and through-bond J_{PP} coupling in a rigid nonsymmetrical bis(phosphine) and its metal complexes. *Inorg. Chem.* **2018**, *57*, 3387–3398.

7 Hierso, J.-C. Indirect Nonbonded Nuclear Spin–Spin Coupling: A Guide for the Recognition and Understanding of "Through-Space" NMR J Constants in Small Organic, Organometallic, and Coordination Compounds. *Chem. Rev.* **2014**, *114*, 4838–4867.

8 (a) Hierso, J.-C.; Fihri, A.; Ivanov, V. V.; Hanquet, B.; Pirio, N.; Donnadieu, B.; Rebière, B.; Amardeil, R.; Meunier, P. "Through-Space" Nuclear Spin−Spin J_{pp} Coupling in Tetraphosphine Ferrocenyl Derivatives: A ^{31}P NMR and X-ray Structure Correlation Study for Coordination Complexes. *J. Am. Chem. Soc.* **2004**, *126*, 11077–11087; (b) Hierso, J.-C.; Evrard, D.; Lucas, D.; Richard, P.; Cattey, H.; Hanquet, B.; Meunier, P. Through-space" ^{31}P spin–spin couplings in ferrocenyl tetraphosphine coordination complexes: Improvement in the determination of the distance dependence of J_{PP} constants. *J. Organomet. Chem.* **2008**, *693*, 574–578 ; (c) Smaliy, R. V.; Beaupérin, M.; Cattey, H.; Meunier, P.; Hierso, J.-C. Conformational Control of Metallocene Backbone by Cyclopentadienyl Ring Substitution: A New Concept in Polyphosphane Ligands Evidenced by "Through-Space" Nuclear Spin−Spin Coupling. Application in Heteroaromatics Arylation by Direct C−H Activation. *Organometallics* **2009**, *28*, 3152–3160; (d) Mom, S.; Beaupérin, M.; Roy, D.; Royer, S.; Amardeil, R.; Cattey, H.; Doucet, H.; Hierso, J.-C. Congested Ferrocenyl Polyphosphanes Bearing Electron-Donating or Electron-Withdrawing Phosphanyl Groups: Assessment of Metallocene Conformation from NMR Spin Couplings and Use in Palladium-Catalyzed Chloroarenes Activation. *Inorg. Chem.* **2011**, *50*, 11592–11603.

[9] (a) Kimber, B. J.; Feeney, J.; Roberts, G. C. K.; Birdsall, B.; Griffiths, D. V.; Burgen, A. S. V.; Sykes, B. D. Proximity of two tryptophan residues in dihydrofolate reductase determined by ^{19}F NMR. *Nature*, **1978**, *271*, 184–185; (b) Arnold, W. D.; Mao, J.; Sun, H.; Oldfield, E. Computation of Through-Space ^{19}F–^{19}F Scalar Couplings via Density Functional Theory. *J. Am. Chem. Soc.* **2000**, *122*, 12164–12168; (c) Malkina, O. L.; Malkin V. G. Visualization of Nuclear Spin–Spin Coupling Pathways by Real- Space Functions. *Angew. Chem. Int. Ed.* **2003**, *42*, 4335–4338.

[10] Beaupérin, M.; Smaliy, R.; Cattey, H.; Meunier, P.; Ou, J.; Toy, P. H.; Hierso, J.-C. Modular functionalized polyphosphines for supported materials: previously unobserved ^{31}P-NMR «through-space» ABCD spin systems and heterogeneous palladium-catalysed C–C and C–H arylation. *Chem. Commun.* **2014**, *50*, 9505–9508.

[11] (a) Nguyen, T.-A.; Roger, J.; Nasrallah, H.; Rampazzi, V.; Fournier, S.; Cattey, H.; Fleurat-Lessard, P.; Devillers, C. H.; Pirio, N.; Lucas, D.; Hierso, J.-C. Gold(I) Complexes Nuclearity in Constrained Ferrocenyl Diphosphines: Dramatic Effect in Gold-Catalyzed Enyne Cycloisomerization. *Chem. Asian J.* **2020**, *15*, 2879–2885; (b) Rampazzi, V.; Roger, J.; Amardeil, R.; Penouilh, M.-J.; Richard, P.; Hierso, J.-C. Gold(I) Complexes of Ferrocenyl Polyphosphines: Aurophilic Gold Chloride Formation and Phosphine-Concerted Shuttling of a Dinuclear [ClAu···AuCl] Fragment. *Inorg. Chem.* **2016**, *55*, 10907−10921.

[12] (a) Yam, V. W.-W.; Chan, C.-L.; Choi, S. W.-K.; Wong, K. M.-C.; Cheng, E. C.-C.; Yu, S.-C.; Ng, P.-K.; Chan W.-K.; Cheung, K.-K. Synthesis, photoluminescent and electroluminescent behaviour of four-coordinate tetrahedral gold(i) complexes. *Chem. Commun*. **2000**, 53–54; (b) Osawa, M.; Aino, M.-A.; Nagakura, T.; Hoshino, M.; Tanaka, Y.; Akita, M. Near-unity thermally activated delayed fluorescence efficiency in three- and four-coordinate Au(I) complexes with diphosphine ligands. *Dalton Trans.* **2018**, *47*, 8229–8239; (c) Osawa, M.; Yamayoshi, H.; Hoshino, M.; Tanaka, Y.; Akita, M. Luminescence color alteration induced by trapped solvent molecules in crystals of tetrahedral gold(i) complexes: near-unity luminescence mixed with thermally activated delayed fluorescence and phosphorescence. *Dalton Trans.* **2020**, *48*, 9094–9103; (d) Osawa, M.; Soma, S.; Hoshino, M.; Tanaka, Y.; Akita, M. Photoluminescent properties and molecular structures of dinuclear gold(I) complexes with bridged diphosphine ligands: near-unity phosphorescence from ^{3}XMMCT/^{3}MC. *Dalton Trans.* **2020**, *49*, 15204–15212.

[13] (a) Dennis; E. K.; Kim, J. H.; Parkin, S.; Awuah, S. G.; Garneau-Tsodikova, S. Distorted Gold(I)–Phosphine Complexes as Antifungal Agents. *J. Med. Chem.* **2020**, *63*, 2455–2469; (b) Kim, J. H.; Reeder, E.; Parkin, S.; Awuah, S. G. Gold(I/III)-Phosphine Complexes as Potent Antiproliferative Agents. *Sc. Reports*, **2019**, *9*, 12335–12353.

[14] Carvajal, M. A.; Novoa, J. J.; Alvarez, S. Choice of Coordination Number in d10 Complexes of Group 11 Metals. *J. Am. Chem. Soc.* **2004**, *126*, 1465–1477.

[15] Roemer, M.; Heinrich, D.; Kang, Y. K.; Chung, Y. K.; Lentz, D. Bulky-Alkyl-Substituted Bis(trifluorovinyl)ferrocenes: Redox-Autocatalytic Formation of Fluorinated Ferrocenophanes. *Organometallics* **2012**, *31*, 1500–1510.

[16] Inkpen, M. S.; Du, S.; Driver, M.; Albrecht, T.; Long, N. J. Oxidative purification of halogenated ferrocenes. *Dalton Trans.* **2013**, *42*, 2813−2816.

[17] Diphosphines are obtained as side-products in about 20%, which could be isolated from remaining unconverted **2** that is can be also reused for synthesis.

[18] Roger, J.; Royer, S.; Cattey, H.; Savateev, A.; Smaliy, R. V.; Kostyuk, A. N.; Hierso, J.-C. Dialkylated Bis(phosphino) Ferrocenes: Diastereoselective Synthesis and Effects on Silver-Mediated Nucleophilic Fluorination of Chloroquinolines at C–Cl Bond. *Eur. J. Inorg. Chem.* **2017**, 330–339.

[19] Smaliy, R. V.; Beaupérin, M.; Mielle, A.; Richard, P.; Cattey, H.; Kostyuk, A. N.; Hierso, J.-C. Hexaphosphine: A Multifaceted Ligand for Transition Metal Coordination. *Eur. J. Inorg. Chem.* **2012**, 1347−1352.

[20] (a) Peralta, J. E.; Barone, V.; Contreras, R. H. Through-Bond and Through-Space J_{FF} Spin−Spin Coupling in Peridifluoronaphthalenes: Accurate DFT Evaluation of the Four Contributions. *J. Am. Chem. Soc.* **2001**, *123*, 9162–9163; (b) Peralta, J. E.; Barone, V.; RuÍz de Azúa, M. C.; Contreras, R. H. Finite perturbation theory-density functional theory calculation of the spin-dipolar contribution to NMR spin-spin coupling constants. *Mol. Phys.* **2001**, *99*, 655–661; (c) Peralta, J. E.; Barone, V.; Contreras, R. H. Through-Bond and Through-Space J_{FF} Spin−Spin Coupling in Peridifluoronaphthalenes: Accurate DFT Evaluation of the Four Contributions. *J. Am. Chem. Soc.* **2001**, *123*, 9162–9163; (d) For an example involving a simple C–H bond, see: Hierso, J.-C. Nonbonded Indirect Nuclear Spin–Spin Couplings (*J* Couplings ‘‘Through-Space’’) for Structural Determination in *Small Organic and Organometallic Species, in High Resolution NMR Spectroscopy*, ed. R. H. Contreras, Elsevier, Amsterdam, **2013**, p. 285 and ref. therein. Removal of electron density brought about by attachment of an electronegative substituent to carbon atom increases the effective “nuclear charge” of this atom. This perturbation augments the probability of the valence *s* electrons for nuclear contact. Therefore, an increase of the $^1J_{C–H}$ results: the family of chloroalkanes CH_3Cl, CH_2Cl_2 and $CHCl_3$ have $^1J_{C–H}$ SSCCs values of 147 Hz, 177 Hz, and 208 Hz, respectively, while $^1J_{C–H}$ is found in CH_4 to be 125 Hz.

[21] Wagner, J. P.; Schreiner, P. R. London Dispersion in Molecular Chemistry-Reconsidering Steric Effects. *Angew. Chem. Int. Ed.* **2015**, *54*, 12274–12296.

[22] Ernst, L.; Ibrom, K. A New Quantitative Description of the Distance Dependence of Through- Space ^{19}F,^{19}F Spin–Spin Coupling. *Angew. Chem., Int. Ed.* **1995**, *34*, 1881−1882.

[23] Mallory, F. B.; Mallory, C. W.; Butler, K. E.; Lewis, M. B.; Xia, A. Q.; Luzik, E. D.; Fredenburgh, L. E.; Ramanjulu, M. M.; Van, Q. N.; Francl, M. M.; Freed, D. A.; Wray, C. C.; Hann, C.; Nerz-Stormes, M.; Carroll, P. J.; Chirlian, L. E. Nuclear Spin−Spin Coupling via Nonbonded Interactions. 8.[1] The Distance Dependence of Through-Space Fluorine−Fluorine Coupling. *J. Am. Chem. Soc.* **2000**, *122*, 4108–4116.

[24] (a) Gimeno, M. C.; Jones, P. G.; Laguna, A.; Sarroca, C. Synthesis of Silver(I) Complexes with 1,1′-Bis(Diphenyl-Phosphino)Ferrocene (Dppf). Crystal Structures of $[Ag(Dppf)(PPh_3)]ClO_4 \cdot 2CH_2Cl_2$, $[Ag(Dppf)_2]ClO_4 \cdot 2CHCl_3$ and $[Ag(Dppf)(Phen)]ClO_4$(Phen = 1,10-Phenanthroline). *J. Chem. Soc., Dalton Trans.* **1995**, *9*, 1473–1481. (b) Long, N. J.; Martin, J.; Opromolla, G.; White, A. J. P.; Williams, D. J.; Zanello, P. Synthesis and Characterisation of 1-(Diphenylphosphino)-1′-(Methylsulfanyl)Ferrocene and a Series of Metal (CuI, AgI)–Ferrocenylene Complexes. *J. Chem. Soc., Dalton Trans.* **1999**, *12*, 1981–1986. (c) Lu, X. L.; Leong, W. K.; Andy Hor, T. S.; Goh, L. Y. Coordination Polymers and Supramolecular Structures in Ag(I)Triflate–Dppf Systems (Dppf=1,1′-Bis(Diphenylphosphino)Ferrocene). *J. Organomet. Chem.* **2004**, *689*, 1746–1756.

[25] Schmidbaur, H. The aurophilicity phenomenon: A decade of experimental findings, theoretical concepts and emerging applications. *Gold Bulletin*, **2000**, *33*, 3–10.

[26] M. Roemer, D. Heinrich, Y. K. Kang, Y. K. Chung, D. Lentz *Organometallics* **2012**, *31*, 1500–1510.

[27] Gaussian 16, Revision B.01, Frisch, M. J.; Trucks, G. W.; Schlegel, H. B.; Scuseria, G. E.; Robb, M. A.; Cheeseman, J. R.; Scalmani, G.; Barone, V.; Petersson, G. A.; Nakatsuji, H.; Li, X.; Caricato, M.; Marenich, A. V.; Bloino, J.; Janesko, B. G.; Gomperts, R.; Mennucci, B.; Hratchian, H. P.; Ortiz, J. V.; Izmaylov, A. F.; Sonnenberg, J. L.; Williams-Young, D.; Ding, F.; Lipparini, F.; Egidi, F.; Goings, J.; Peng, B.; Petrone, A.; Henderson, T.; Ranasinghe, D.; Zakrzewski, V. G.; Gao, J.; Rega, N.; Zheng, G.; Liang, W.; Hada, M.; Ehara, M.; Toyota, K.; Fukuda, R.; Hasegawa, J.; Ishida, M.; Nakajima, T.; Honda, Y.; Kitao, O.; Nakai, H.; Vreven, T.; Throssell, K.; Montgomery, J. A., Jr.; Peralta, J. E.; Ogliaro, F.; Bearpark, M. J.; Heyd, J. J.; Brothers, E. N.; Kudin, K. N.; Staroverov, V. N.; Keith, T. A.; Kobayashi, R.; Normand, J.; Raghavachari, K.; Rendell, A. P.; Burant, J. C.; Iyengar, S. S.; Tomasi, J.; Cossi, M.; Millam, J. M.; Klene, M.; Adamo, C.; Cammi, R.; Ochteski, J. W.; Martin, R. L.; Morokuma, K.; Farkas, O.; Foresman, J. B.; Fox, D. J. Gaussian, Inc., Wallingford CT, 2016.

[28] Becke, A. D. Density-functional thermochemistry. III. The role of exact exchange. *J. Chem. Phys.* **1993**, *98*, 5648–5652.

[29] Grimme, S.; Ehrlich, S.; Goerigk, L. Effect of the damping function in dispersion corrected density functional theory. *J. Comp. Chem*. **2011**, *32*, 1456–1465.

[30] (a) Lefebvre, C.; Rubez, G.; Khartabil, H.; Boisson, J.-C.; Contreras-García, J.; Hénon, E. Accurately Extracting the Signature of Intermolecular Interactions Present in the NCI Plot of the Reduced Density Gradient versus Electron Density. *Phys. Chem. Chem. Phys.* **2017**, *19*, 17928–17936. (b) Lefebvre, C.; Khartabil, H.; Boisson, J.-C.; Contreras-Garcia, J.; Piquemal, J.-P.; Hénon, E. Independent Gradient Model: A New Approach for Probing Strong and Weak Interactions in Molecules from Wave Function Calculations. *ChemPhysChem* **2018**, *19*, 724–735.

[31] Spackman, P. R.; Turner, M. J.; McKinnon, J. J.; Wolff, S. K.; Grimwood, D. J.; Jayatilaka, D.; Spackman, M. A. CrystalExplorer: A Program for Hirshfeld Surface Analysis, Visualization and Quantitative Analysis of Molecular Crystals. *J. Appl. Cryst.* **2021**, *54*, 1006–1011.